



HAL
open science

A Novel and Enhanced Calibration of the Tilting Weir as a Flow Measurement Structure

Joseph E Pugh, Subhas Karan Venayagamoorthy, Timothy K Gates, Céline
Berni, Marie Rastello

► **To cite this version:**

Joseph E Pugh, Subhas Karan Venayagamoorthy, Timothy K Gates, Céline Berni, Marie Rastello. A Novel and Enhanced Calibration of the Tilting Weir as a Flow Measurement Structure. *Journal of Hydraulic Engineering*, 2024, 150 (2), pp.04023064. 10.1061/JHEND8.HYENG-13796 . hal-04271608v2

HAL Id: hal-04271608

<https://hal.science/hal-04271608v2>

Submitted on 15 Nov 2023

HAL is a multi-disciplinary open access archive for the deposit and dissemination of scientific research documents, whether they are published or not. The documents may come from teaching and research institutions in France or abroad, or from public or private research centers.

L'archive ouverte pluridisciplinaire **HAL**, est destinée au dépôt et à la diffusion de documents scientifiques de niveau recherche, publiés ou non, émanant des établissements d'enseignement et de recherche français ou étrangers, des laboratoires publics ou privés.

1 **A NOVEL AND ENHANCED CALIBRATION OF THE TILTING WEIR**
2 **AS A FLOW MEASUREMENT STRUCTURE**

3 Joseph E. Pugh¹, S. Karan Venayagamoorthy, PhD², Timothy K. Gates, PhD³, Céline Berni,
4 PhD⁴, and Marie Rastello, PhD⁵

5 ¹PhD Candidate, Environmental Fluid Mechanics Laboratory, Dept. of Civil and Environmental
6 Engineering, Colorado State University, 1372 Campus Delivery, Fort Collins, CO, 80523, USA.

7 (corresponding author) Email: jepugh@colostate.edu. ORCID:

8 <https://orcid.org/0000-0002-7959-3958>.

9 ²Professor, Environmental Fluid Mechanics Laboratory, Dept. of Civil and Environmental
10 Engineering, Colorado State University, 1372 Campus Delivery, Fort Collins, CO, 80523, USA.

11 Email: vskaran@colostate.edu. ORCID: <https://orcid.org/0000-0001-7895-4144>.

12 ³Professor, Dept. of Civil and Environmental Engineering, Colorado State University, 1372
13 Campus Delivery, Fort Collins, CO, 80523, USA. Email: tkg@colostate.edu. ORCID:

14 <https://orcid.org/0000-0003-4702-4395>.

15 ⁴Researcher, INRAE, Unit Recherche RiverLy, HHLab, 69100 Villeurbanne, France. Email:

16 celine.berni@inrae.fr. ORCID: <https://orcid.org/0000-0003-1806-7054>.

17 ⁵Researcher, Univ. Grenoble Alpes, CNRS, Grenoble INP, LEGI, 38000 Grenoble, France.

18 Email: marie.rastello@legi.cnrs.fr. ORCID: <https://orcid.org/0000-0002-4457-1433>.

19 **ABSTRACT**

20 A large collection of laboratory measurements of piezometric head (h) and discharge (Q) are
21 made over hydraulic models of a tilting weir at nine different angles, ranging from 25.7° to 90°
22 within a 0.3-m wide flume. These measurements are corroborated with additional laboratory data
23 taken within a 1-m wide flume across four inclination angles. The range of both inclination angle

(θ) and flow scale examined in this study elucidate the nature of the head-discharge rating equation beyond previous work. Results show that as θ decreases under a constant Q , the h over the weir decreases in a monotonic fashion due to the shallower angle of attack of the flow, which results in less curvature of the streamlines over the crest and therefore less deviation from the upstream hydrostatic pressure condition. To incorporate this effect into the head-discharge rating equation, a transformation of the h term is applied by multiplying the measured h that occurs over a tilting weir by a correction factor to match the effective h that would occur if the weir were aligned perpendicular to the flow at the same discharge. Thus, a modified form of the classical sharp-crested weir rating equation can be used as a means for determining the value of Q for tilting cases to a high degree of accuracy. The degree of accuracy is dependent upon dimensionless Reynolds and Weber numbers describing the flow inertia in the approach to the weir in relation to respective viscous and surface tension scale effects. This approach portends marked flow measurement enhancement for flow conditions above a suggested inertial threshold.

PRACTICAL APPLICATIONS

To achieve reliable and equitable water distribution it is necessary to accurately estimate the volumetric discharge of water flow through rivers and channels. One such method of accomplishing this is by using hydraulic structures, such as the tilting weir. This structure not only can be used to measure the discharge of water on a continuous basis, but also allows for regulating the water level upstream of the structure. Presently, tilting weirs are often used to control water levels, but the literature on their utilization as flow measurement structures has remained sparse. This study presents a thorough analysis of laboratory experiments on scaled models of tilting weirs, where the flow depth upstream of the structure and the inclination angle are used to calibrate an equation to estimate the discharge to a high degree of accuracy. Operational guidelines to ensure minimum uncertainty in measurement are also given.

INTRODUCTION

Tilting weirs (i.e. overshoot gates or pivot weirs) have been in use since the late twentieth century for the purpose of regulating upstream water levels in open channel flow, typically within

51 the context of irrigation systems or spillway operation (Wahlin and Replogle 1994; Stringam and
52 Gill 2012; Lee et al. 2014; Bijankhan and Ferro 2017). These simple overflow structures operate as
53 a flat rectangular plate that is hinged to the bottom of the channel and inclined from the horizontal
54 through the use of pneumatic pressure vessels, a pulley mechanism, or a piston mechanism. It is
55 generally assumed that the crest of these structures is thin, so that a springing jet (i.e. nappe) forms
56 on the downstream side of the structure. In irrigation systems, tilting weirs allow for regulation
57 of the stage upstream of the structure to provide the pressure head necessary to divert flow from
58 a main supply canal into lateral canals. In spillway operation, these structures can be installed in
59 parallel to allow for careful release of flows and regulation of the reservoir stage in response to
60 varying supply and demand levels.

61 Tilting weirs require careful consideration of aeration demands for the underside of the plunging
62 nappe to be supported by atmospheric pressure (Bos 1976). If these structures are properly
63 designed, the downstream channel bed elevation will be set low enough to allow for the energy of
64 the supercritical plunging nappe to be dissipated, while also ensuring that a sufficient supply of
65 fresh air is provided to the pocket of atmospheric pressure supporting the nappe. For these reasons,
66 tilting weirs offer the potential of being practical hydraulic structures that serve the dual functions
67 of stage regulation and discharge measurement. The initial development of these structures as stage
68 regulation devices has been well documented and widely implemented (Clemmens et al. 2001;
69 Floodlist News 2017). However, their use as flow measurement devices remains in need of further
70 investigation.

71 **Fundamentals of the Weir Rating Equation**

72 The development of a method for predicting the volumetric discharge over tilting weirs begins
73 with an understanding of Torricelli's principle of a jet at the base of a reservoir issuing from a
74 small orifice. Here, the velocity (u) of the jet can be related to the potential energy in the static
75 supply reservoir by the function $u = \sqrt{2gh}$, with h being the elevation of the water surface above
76 the jet outlet. This principle assumes the flow is inviscid and irrotational, and that the pressure
77 distribution over the crest is hydrostatic. In his 1717 publication "de moto aquae mixto", Giovanni

78 Poleni applied Torricelli's principle to approximate the discharge of a fluid over a perpendicular
79 weir as occurring in a series of horizontal elements, the velocity of each being proportional to
80 the distance of the fluid element from the free surface (Rouse and Ince 1963). From the resultant
81 parabolic velocity profile, the depth-integrated unit discharge (q) can be approximated using what
82 is known as Poleni's equation.

$$83 \int_0^h u \, dh \approx \frac{2}{3} \sqrt{2gh} h^{3/2} \approx q \quad (1)$$

84 However, it is known that because of the simplifying assumptions implicit in Eq. 1, a dimen-
85 sionless correction factor must be applied to the idealized efflux to account for the contraction of
86 jet at the crest of the orifice. This has typically been called the discharge coefficient (C_d) when
87 referring to weir flow, but it is in effect a coefficient of contraction (Kindsvater and Carter 1957).
88 Its application to Eq. (1), with the addition of the crest length (b) to account for the transversal
89 dimension, then yields the standard volumetric discharge rating equation for a sharp-crested weir.

$$90 Q = C_d \frac{2}{3} \sqrt{2gb} h^{3/2} \quad (2)$$

91 This relatively simple equation forms the theoretical basis for the discharge equation of dif-
92 ferent types of sharp-crested weirs with variable geometries (Martínez et al. 2005). However, the
93 simplifying assumptions of this approach should not be overlooked. As previously mentioned, this
94 derivation approximates the flow between the upstream head measurement location and the crest
95 as being inviscid, irrotational, and hydrostatic. For the case of accelerating flow over a weir, it is
96 often taken to be a safe assumption that over the short reach from the measurement section to the
97 crest, the energy loss due to internal rotational shear is negligible (Kindsvater and Carter 1957).

98 The assumptions of inviscid flow and a hydrostatic pressure distribution can be best examined
99 by considering the theoretical case of a sharp-crested weir of infinite height. Here the assumption of
100 potential flow is valid because the effect of the boundary is negligible. For this case, the streamlines
101 will approach the crest radially so that a significant vertical velocity component will be present
102 in the flow. This causes the pressure distribution to decrease significantly from the hydrostatic

103 condition. This pressure drop correspondingly results in an acceleration of the flow over the crest
104 and a reduction in the depth of flow at the crest to satisfy the continuity principle (Rouse 1932).
105 The contraction coefficient of the water surface profile over the crest of an infinitely high weir has
106 been shown from potential flow theory to be equal to Kirchhoff's coefficient for a jet issuing from
107 a sharp-edged orifice, where $C_d = \frac{\pi}{\pi+2} = 0.611$ (Rouse 1946b).

108 If a low weir is considered, so that the effect of the boundary cannot be neglected and the
109 assumption of inviscid flow no longer holds, it can be observed that the flow separates near the
110 base of the weir and a standing eddy forms. This phenomenon was briefly verified in this study by
111 preliminary particle-image velocimetry analysis, as shown by Fig 1. A boundary layer is present
112 due to viscous effects causing a deceleration of the flow near the channel bed, as well as the
113 upstream face of the weir. The magnitude of these respective boundary layers can be described
114 by the boundary-layer displacement-thickness (δ^*) (Kindsvater and Carter 1957). The effect of
115 the flow separation on the streamlines upstream of the weir was described by Rouse (1932) as
116 being akin to tilting the weir downstream, due to the fact that the streamlines above the separation
117 zone retain more horizontal momentum. This results in less curvature of the streamlines at the
118 crest and less contraction of the overflowing jet, so that the pressure at the vena contracta more
119 closely approximate the hydrostatic condition. The result is that for a low weir, more discharge can
120 be passed given the same upstream energy condition compared to that for an infinitely high weir
121 (Rouse 1932).

122 **Dimensional Analysis**

123 If the assumption is made that the tilting weir can be treated as a modified case of the classical
124 sharp-crested weir, the general form of Eq. (2) can be applied to establish a head-discharge rating
125 equation for the tilting weir by adding a term that accounts for the inclination angle (θ) of the
126 weir with respect to the horizontal. In order to understand the relevant flow parameters and fluid
127 properties that influence this equation, a dimensional analysis of the tilting weir is now considered.

128 Simplifying assumptions are made that the weir crest length (b) is equal to the width of the
129 approach channel (B), and the velocity field is uniform in the transversal direction. The flow

130 geometry can then be described by the parameters shown in Fig. 2. Here, L is the vertical height
 131 of one weir when positioned perpendicular to the channel bed; p is the elevation of the weir crest
 132 above the channel bed at a given θ ; and h is the piezometric head measured with reference to the
 133 crest elevation in the uniform flow section upstream from the weir. The total hydraulic head (H), is
 134 the sum of the piezometric head (h) and the kinetic energy head ($\alpha \bar{U}^2/2g$), where \bar{U} is the velocity
 135 averaged over the channel cross section in the approach, α is the kinetic energy correction factor,
 136 and g is the gravitational acceleration. The dimensionless term, $\sin \theta = p/L$ describes the effect
 137 that the changing angle of attack of the flow on the weir has on the streamlines over the crest,
 138 and relates p and L . The relevant fluid properties in determining the flow over the weir are the
 139 density, ρ , the dynamic viscosity, μ , and surface tension, σ . Since this is a case of open channel
 140 flow, gravitational effects are critical and thus g is included as a relevant physical parameter. A
 141 functional description of the unit discharge over a fully-suppressed ($b/B = 1$) tilting weir can be
 142 written as:

$$143 \quad q = f(p, h, \sin \theta, g, \rho, \mu, \sigma) \quad (3)$$

144 Utilizing Buckingham π analysis and a yet to be determined function (ϕ), the following dimension-
 145 less equation can be written using the scaling terms $h \equiv L$, $h/\sqrt{gh} \equiv T$, and $\rho h^3 \equiv M$:

$$146 \quad C_d = \frac{3}{2\sqrt{2}} Fr = \phi(h/p, \sin \theta, Re, We) \quad (4)$$

147 wherein:

$$148 \quad Fr = \frac{q}{\sqrt{gh}^3/2} \quad (5)$$

$$149 \quad Re = \frac{\sqrt{gh}^3/2}{\nu} \quad \text{where } \nu = \mu/\rho \quad (6)$$

$$150 \quad We = \frac{\rho gh^2}{\sigma} \quad (7)$$

153 The first term in Eq. (4) is the classical discharge coefficient as shown in Eq. (2), which can be
 154 considered as a dimensionless Froude number (Fr) for the flow over the weir crest ($q/\sqrt{gh}^3/2$),

155 that has then been transformed by the coefficient $3/2\sqrt{2}$ to make the inertial term in the numerator
156 reflect the depth-averaged velocity from Poleni's approach in Eq. (1).

157 Regimes of flow over a weir can be divided into four types: clinging, laminar, free, and inundated
158 flow (Johnson 1996; Sinclair et al. 2022). These regimes and their respective effect on the shape
159 of the nappe were first described by Bazin (1898), and later summarized by Rao (1975). When the
160 flow over the weir is clinging, its inertia is not sufficient to overcome scale effects due to surface
161 tension. Here, the free surface clings to the weir plate and the nappe downstream of the crest is
162 not fully formed. This causes the same discharge to pass over the weir at a lower head compared
163 to when the nappe is fully formed, thus artificially increasing the discharge coefficient (Sarginson
164 1972). An additional flow regime can occur at low heads, even when the nappe is no longer
165 clinging to the downstream face. This flow regime has also been described as a depressed nappe
166 (Rao 1975). Here, viscous effects rather than surface tension effects are dominant. The flow inertia
167 is not sufficient to overcome viscous effects in the same manner that is observed within the free
168 flow regime; hence the velocity profile deviates from that expected for turbulent open-channel flow
169 (Rouse 1946a). This reduction in the upstream bulk velocity causes h over the weir to artificially
170 increase in order to satisfy conservation of mass, thus decreasing C_d below what is expected for the
171 free flow relationship (Schoder and Turner 1929). Inundated flow occurs on the opposite end of the
172 inertial spectrum, but the effect on C_d is nominally the same as for clinging flow. Here, the pressure
173 head above the weir becomes too great for the air pocket beneath the nappe to be sustained, the
174 nappe collapses, and the head over the weir decreases. Free flow then occurs in between the limits
175 of clinging/laminar and inundated flow, when the weir is operating within the conditions assumed
176 in Eq. (2). This means that dynamic similarity is present so that the flow dynamics are independent
177 of viscous and surface tension scale effects, and that the nappe downstream of the crest is fully
178 supported by a fresh supply of air at atmospheric pressure.

179 If viscous and surface tension effects are taken to be negligible within the normal operating
180 parameters of the weir, then determining the head-discharge equation over a tilting weir converges
181 upon an understanding of how C_d behaves as a function of the dynamic parameters h/p and $\sin \theta$.

182 As Rouse (1932) speculated, the reduction in $\sin \theta$ is likely to have the same effect as increasing
183 the h/p ratio, by which the streamlines become more horizontal over the crest and the contraction
184 coefficient increases to allow more discharge over the weir, given the same upstream head condition.
185 The goal of this study is to determine the behavior of the discharge capacity of a tilting weir as it
186 relates to h/p and $\sin \theta$, as well as the range of Reynolds number (Re) and Weber number (We)
187 values that can be considered as a normal operating regime for free flow.

188 REVIEW OF PREVIOUS WORK

189 Sharp-Crested Weirs

190 Much careful experimental work was completed on the flow measurement equation for sharp-
191 crested weirs from the late-nineteenth until the mid-twentieth century to find an empirical equation
192 to relate C_d (as in Eq. 4) to h/p under normal operating conditions, *i.e.* when Re and We effects
193 can be neglected. Notable works on this topic are those of Smith (1886), Bazin (1898), Rafter
194 (1900), Horton (1906), Schoder and Turner (1929), Rehbock (1929), and USBR (1948).

195 A seminal work on the topic that aimed to integrate the work of previous researchers, while
196 offering a large amount of new experimental data, was that of Kindsvater and Carter (1957). These
197 researchers at Georgia Tech University offered the novel contribution of taking into consideration
198 viscous and surface tension effects that become relevant at low values of h . They also considered the
199 effect on the flow dynamics for weirs where $b/B < 1$. Kindsvater and Carter (1957) convincingly
200 showed that earlier formulas for C_d in Eq. (4) of a nonlinear form were overly complex, and that a
201 simple linear equation could be used instead. They also suggested the use of empirically calibrated
202 correction factors, k_h and k_b to account for Re and We scale effects under small values of h and
203 b , introducing equivalent head (h_e) and equivalent crest length (b_e) terms to obtain an effective
204 discharge coefficient (C_e) for sharp-crested weirs:

$$205 \quad C_e = \frac{Q}{\frac{2}{3}\sqrt{2g}b_e h_e^{3/2}} \approx 0.602 + 0.075h/p \quad (8)$$

with

$$h_e = h + k_h \quad (9)$$

$$b_e = b + k_b \quad (10)$$

The authors recommended the use of a k_h value of 0.003 ft, or approximately 1 mm. The use of k_h is important only when values of h are small. For water flow through air, [Kindsvater and Carter \(1957\)](#) estimated that prediction error due to viscous and surface tension effects would be within 2% as long as $h > 0.06$ m. It was also emphasized that k_h is an empirically calibrated correction factor that could differ significantly depending on which set of experimental data was used. The original authors attributed this to differences in experimental equipment. However, we hypothesize that this discrepancy may be due to the fact that at low values of h , either We or Re effects can be dominant depending on whether the nappe is fully formed or not. Evidence for this bifurcation in the flow behavior at low h is given in [Zhang et al. \(2010\)](#). By giving k_h as a positive parameter, [Kindsvater and Carter \(1957\)](#) implicitly assumed We effects to be dominant at low values of h , as explained earlier. Therefore, the specific choice of k_h may be a point in need of finer calibration on a case by case basis, but we report here the recommended value $k_h = 0.001$ m of the original authors. A less uncertain choice is the value of k_b . [Kindsvater and Carter \(1957\)](#) found little variability in the value of this parameter within the experimental data they examined, likely because it is a function of the static contraction ratio parameter, and not the dynamic variable h . They recommended a k_b value of -0.003 ft (-0.001 m) for the case where $b/B = 1$.

After the work of [Kindsvater and Carter \(1957\)](#), several other publications have further elucidated the nature of sharp-crested weir flow over a wide range of h/p values, including measurements of velocity and pressure distributions near the crest. ([Rajaratnam and Muralidhar 1971](#); [Ramarathnam et al. 1987](#); [Swamee 1988](#); [Sinclair et al. 2022](#)).

Tilting Weirs

With the early explorations of the sharp-crested weir as a flow measurement device, examinations were also made to investigate the effect that tilting the upstream face of the weir had on the

233 nappe profiles, and on the head over the crest at a constant discharge (Bazin 1898; USBR 1948;
234 Abou Seida and Quaraishi 1976). Hager (1994) compiled the data from several of these types of
235 studies to develop a flow-rating equation for tilting weirs of the form:

$$236 \quad Q = \left[\frac{2}{3} C_e + 0.05 \sin \left(\frac{3}{2} (90 - \theta) \right) \right] b \sqrt{2g} h^{3/2} \quad (11)$$

237 where C_e is Eq. 8 of Kindsvater and Carter (1957), the effective discharge coefficient for a sharp-
238 crested weir, and θ is in degrees. The second term in the brackets on the right hand side of Eq.
239 11 accounts for the effect of the changing θ on the overall discharge capacity of the structure.
240 This study, published in German, represents an interesting first investigation into the flow-rating
241 equation of a tilting weir. However, it was limited by the fact that the early experimental studies
242 cited by Hager (1994) and used for calibration did not cover a wide range of flow conditions (i.e.
243 h/p values).

244 The seminal work to date attempting to develop a flow-rating equation for tilting weirs is that
245 of Wahlin and Replogle (1994). The authors of this technical report studied two models in a large
246 flume ($B = 1.2$ m). As predicted earlier by Rouse (1932), they began with the assumption that the
247 general form of the sharp-crested weir rating equation as given by Kindsvater and Carter (1957) in
248 Eq. (8), could be applied to the modified case of the tilting weir with the addition of a corrective
249 factor to account for variation in θ . They chose to call this term C_a . By studying data previously
250 collected by the US Bureau of Reclamation (USBR) in analysis of the nappe profiles for flow over
251 variously inclined weirs (USBR 1948), the authors hypothesized that the relation between C_a and
252 θ would take the form of a second order concave polynomial. C_a can also be thought of as a
253 discharge amplification factor, Q_θ/Q_{90} , which represents the relative effect of θ on the amount of
254 discharge that is able to pass over the structure at a given head, compared to the perpendicular 90°
255 case. The results of the study proved to be fairly true to the original hypothesis, and a second order
256 polynomial was defined as: $C_a = 1.0333 + 0.003848\theta - 0.000045\theta^2$, with θ in degrees. Although
257 by definition C_a should be unity when $\theta = 90^\circ$, the authors did not verify this experimentally, and

258 their empirical equation for C_d does not reflect this.

259 Furthermore, the number of observations in their study for $\theta > 45^\circ$ were limited. For $\theta = 54.2^\circ$,
260 14 data points were collected over an h/p range of 0.11-0.3 ($0.04 < h < 0.11$ m), and for $\theta = 63.4^\circ$
261 only seven observations were made over an h/p range of 0.09-0.22 ($0.03 < h < 0.09$ m). With such
262 small values of h , the observations may have been subject to We and Re scale effects (Rehbock
263 1929; Kindsvater and Carter 1957). Thus, it is a concern of the current authors as to whether
264 applying the inclination-angle correction factor given by Wahlin and Replogle (1994) for $\theta > 45^\circ$ is
265 advisable. Wahlin and Replogle (1994) did report that when using their approach for $20^\circ < \theta < 45^\circ$,
266 an average percent error of only 0.8% was found in their predictions of the laboratory data. At
267 the very least, this means there was low prediction bias for their approach within this range of θ .
268 From the experimental data published in the appendix of the study, the current authors computed
269 the mean absolute value percent error (MAPE) to be 2.5% for this same case, which gives a more
270 complete understanding of the magnitude of residual error from this approach. When applying
271 the laboratory-derived equation to a field-scale structure, it was found that their equation under-
272 predicted the discharge in the field by an average of 6.34% (Wahlin and Replogle 1994). This raises
273 the question of how directly applicable laboratory-calibrated discharge-rating equations are to field
274 conditions (Hajimirzaie and González-Castro 2021).

275 Since the first study of Wahlin and Replogle (1994) little convergence has been observed in
276 the published experimental data on flow over the tilting weir. Prakash et al. (2011) conducted a
277 laboratory experiment of flow over inclined rectangular notched weirs, with $\theta = 30^\circ, 45^\circ, 60^\circ,$
278 $75^\circ,$ and 90° . They found that the discharge capacity of the structure increases as θ decreases,
279 and proposed an equation containing two fourth-order polynomials to account for this effect that
280 was accurate to within 10%. However, the authors did not validate their findings with previous
281 experimental data for flow over sharp-crested weirs, and their data have since found little agreement
282 with results published by subsequent authors.

283 Work completed in South Korea has focused on studying the flow characteristics of free and
284 submerged flow over tilting weirs, as well as how sedimentation patterns are affected by the

285 inclination angle of the weir (Lee et al. 2014; Lee 2016; Lee 2018). These works have suggested
286 incorporating the upstream total hydraulic head (H) into the tilting weir rating equation in order
287 to model the effect of θ on the flow. However, this suggestion does not offer the most practical
288 means of implementation in the field, where measuring the kinetic energy head in the approach
289 channel is difficult. Unfortunately, these works have also yet to be published in English; thus their
290 applicability to the wider engineering community remains obscure.

291 Nikou et al. (2016) investigated tilting weirs in a laboratory setting with different side contrac-
292 tions for $\theta = 20^\circ, 40^\circ, 60^\circ, 80^\circ,$ and 90° . However, these authors made their observations over only
293 a small number of discharge scenarios, which resulted in calibration of the empirical coefficients
294 to only $\pm 15\%$ in prediction accuracy. Additionally, in a discussion piece, Khalili Shayan et al.
295 (2018) convincingly showed that the assumption of the original authors that critical flow occurs
296 over the weir crest was inaccurate.

297 Bijankhan and Ferro (2018) attempted to develop a rating equation for the tilting weir that
298 was meant to be independent of the dynamic head over the structure as measured by h/p . This
299 form is simpler in the sense that it depends on fewer parameters, but also less accurate because
300 it neglects how C_d increases linearly with h/p (Kandaswamy and Rouse 1957). Furthermore,
301 Bijankhan and Ferro (2018) did not explain how a fresh air supply was provided underneath the
302 nappe to ensure the condition of atmospheric pressure. From the experimental photos published
303 by the authors, it appears the flow was not sufficiently aerated and thus subject to inundation
304 effects, especially at low θ values where the relative difference between the crest elevation and
305 tailwater depth is small. Furthermore, in a discussion piece on a follow-up study that Bijankhan
306 and Ferro (2020) completed over submerged tilting weirs, Hajimirzaie and González-Castro (2021)
307 revealed a flaw in the dimensional analysis of the authors, originally developed by Ferro (2012).
308 This error introduces a spurious correlation between the independent and dependent dimensionless
309 parameters. This leads to the perceived conclusion that C_d , as in Eq. 4, is independent of h/p .
310 Several experimental investigations have shown that this conclusion is incorrect (Kandaswamy and
311 Rouse 1957; Wahlin and Replogle 1994; Sinclair et al. 2022).

312 Other researchers have studied the flow characteristics of tilting weirs using numerical modeling.
313 **Mahdavi and Shahkarami (2020)** utilized smoothed particle hydrodynamics to provide helpful
314 visualizations of the flow field both upstream and downstream of the weir crest. The authors also
315 validated their simulations with good agreement to available data from physical experiments, at
316 least when $\theta = 90^\circ$. However, the authors did not study a sufficiently large number of flow scenarios
317 to accurately calibrate a head-discharge equation dependent on θ . **Khatamipour et al. (2022)** studied
318 Reynolds-averaged Navier-Stokes (RANS) simulations of flow over tilting weirs in Open FOAM
319 using a two-dimensional $k-\epsilon$ turbulence model over 12 flow cases. The authors observed similar
320 behavior to **Wahlin and Replogle (1994)** in the relationship between Q_θ/Q_{90} and θ , but at smaller
321 magnitudes of Q_θ/Q_{90} than the original study. It was also apparent from the published qualitative
322 flow images that the flow was submerged for $\theta < 90^\circ$, and thus not viable for calibrating a free-flow
323 rating equation.

324 Most recently, **Zerihun (2022)** presented a flow-rating equation for tilting weirs derived from
325 first principles using the Boussinesq-type energy equation for depth-averaged flow. This allowed
326 for the creation of a numerical code that accounted for the presence of non-hydrostatic effects in
327 the sub-critical to super-critical transition region near the crest of the tilting weir. The results
328 of the numerical simulations agreed well with the experimental nappe profiles of **Bazin (1898)**
329 and **USBR (1948)**. However, the flow-rating equation presented by **Zerihun (2022)** lacks practical
330 applicability in that it includes terms requiring a priori knowledge of the slope of the free surface
331 and overflowing nappe.

332 To summarize, the consensus on how to properly treat the influence of θ on the flow character-
333 istics of a tilting weir has so far been lacking in the literature. The initially proposed approach of
334 **Wahlin and Replogle (1994)** has not been sufficiently validated for $\theta > 45^\circ$, and the large majority
335 of subsequent work has been lacking in experimental rigor. More recent work on determining the
336 effect of the flow attack angle over other types of weirs has further highlighted that the influence of
337 θ should not be neglected (**Schmocker et al. 2011**). Higher-order approaches, such as that presented
338 by **Zerihun (2022)**, offer promise for further exploration of this problem numerically but remain

339 to be clearly linked to methods for practical implementation. In pursuit of that, we present here a
340 thorough experimental effort at two unique geometric scales that entails a large number of careful
341 observations across all relevant θ and h/p values for channel flow.

342 **EXPERIMENTAL SETUP AND MEASURING DEVICES**

343 Experiments were first conducted in a recirculating flume manufactured by Armfield and located
344 in the Environmental Fluid Mechanics Laboratory (EFML) at Colorado State University (CSU),
345 USA. The flume was 5 m in length and 0.3 m wide, with a smooth neoprene channel bed and
346 glass side walls. The flume slope was set to be horizontal. Beyond the inlet condition provided
347 by the flume manufacturers, it was found necessary to install a honeycomb-like matrix of porous
348 material at the flume inlet to straighten and normalize the incoming flow. Furthermore, a series of
349 small roughness elements were installed just downstream of the honeycomb matrix in order to trip
350 the turbulent boundary layer and reproduce as close as possible a fully-developed open-channel
351 velocity profile. The downstream channel boundary condition was a free-overfall.

352 Nine tilting weir models were constructed at $\theta = 25.7^\circ, 29.1^\circ, 36.4^\circ, 45^\circ, 50^\circ, 53^\circ, 64^\circ, 71.2^\circ,$
353 and 90° by machining two sheets of smooth acrylic plastic of 12.7 mm (0.5 in.) thickness and
354 adhering them together using a waterproof adhesive. The length of the weir plate (L), as shown in
355 Fig. 2, was consistent between all models at 150 mm. The crest of each model was precisely cut
356 to be "knife-edged", with the angle between the downstream-sloping crest and the parallel sides of
357 the acrylic plates being 45° . Due to air entrainment caused by the plunging nappe, circular tubes
358 of PVC plastic were also installed along the glass side walls of the flume to provide access to fresh
359 air supply, as is shown in Fig. 3. This ensured that the air pocket beneath the overflowing nappe
360 was fully aerated to atmospheric pressure. The diameter of these tubes was sized to 19 mm (0.75
361 in.) according to specifications detailed in [Bos \(1976\)](#).

362 Measurements of h and steady Q were made over a full range of flow conditions for each model,
363 ranging from clinging/laminar flow at the minimum, to fully inundated flow at the maximum. At
364 least 20 observations were made within the free-flow regime, where dynamic similarity is achieved
365 and the inertia of the flow is great enough to be free from scale effects caused by viscosity and

366 surface tension, while also avoiding the under-pressurization of the nappe caused by inundated
367 flow (see Table 1). These free-flow observations were used to calibrate C_e as a function of h/p
368 for each model. Observations of h were made at a distance of 0.8 m upstream of the model crest
369 using a vernier-type point gauge to an accuracy of ± 0.3 mm (0.001 ft). Measurement of steady Q
370 through the flume was made using an electromagnetic flow meter located within the supply pipe
371 to the channel with an accuracy of ± 0.3 L/s (0.01 cfs). Measurements of water temperature also
372 were taken, at an accuracy of $\pm 0.1^\circ\text{C}$ in order to precisely calculate temperature-dependent values
373 for μ and σ .

374 To ensure the initial results of the EFML experiments were both reproducible and scalable,
375 follow-up experiments were conducted in a similar recirculating flume located in the Hydraulic
376 and Hydromorphology Laboratory (HHLab) of the RiverLy research unit operating in the centre of
377 the Institut National de Recherche pour l'Agriculture, l'Alimentation, et l'Environnement (INRAE)
378 located in Lyon-Villeurbanne, France. This flume was larger than the EFML flume, at 1 m wide and
379 18 m in length, with a smooth glass channel bottom and side walls (see Fig. 3). These experiments
380 were conducted in the same manner as the earlier EFML experiments, with some minor variations.
381 Here, four tilting weirs of the same design as the EFML models were examined at $\theta = 33^\circ, 44^\circ, 59^\circ,$
382 and 90° , and L was reduced to 126 mm. The crest location of each model structure was kept
383 consistent at 11 m downstream of the flume inlet, which was a sufficiently long entrance length to
384 ensure a fully developed velocity profile. Measurements of h were made 0.8 m upstream of the
385 crest location using a trio of ultrasonic depth sensors measuring at 50 Hz and spaced evenly in the
386 transverse direction across the 1 m wide channel. Measurements of steady Q were made using an
387 electromagnetic flow meter recording at 50 Hz. The resultant time-series of h and Q were then
388 averaged over 60 s to yield mean values, and the measurements of h were further averaged across
389 the three sensors. The standard deviation in the measurements of h and Q were approximately 1
390 mm and 0.3 L/s, respectively.

391 RESULTS

392 Verification with Previous Experimental Work

393 The present goal is to utilize the tilting weir as a special case of the sharp-crested weir ($\theta = 90^\circ$).
394 In the interest of best-practice we choose here to verify our experimental results for the vertical
395 sharp-crested weir, labeled as experiments K and O in Table 1. In Fig. 4, it can be seen that
396 there is excellent agreement between the dimensionless rating equation of **Kindsvater and Carter**
397 **(1957)**, given by Eq. (8), and the experimental data for the sharp-crested weir observed within
398 the current study. For the combined 47 observations shown in Fig. 4, the MAPE between the
399 observed C_e , and that predicted by Eq. (8) is only 0.55 %. Also plotted is the C_e equation given in
400 **Rehbock (1929)**. It corresponds to: $C_e = 0.602 + 0.082(h/p)$. **Rehbock (1929)** recommended the
401 use of this equation with a k_h value of 1.25 mm as a very close alternative to his equation for the
402 "non-effective" discharge coefficient (i.e. $C_d = 0.605 + 0.08h/p$). The **Rehbock (1929)** equation
403 has the same intercept as Eq. (8), but the slope does not match the current experimental data as well
404 as that of **Kindsvater and Carter (1957)**. Because these experiments were completed in relatively
405 narrow channels of width $b = 0.3$ and 1 m, we chose to use the recommended k_b value of 0.001
406 m from **Kindsvater and Carter (1957)** for a full-width ($b/B = 1$) weir in a narrow-width channel.
407 However, we found it unnecessary to implement the introduction of k_h because for our experiments
408 K and O, we did not observe the artificial increase in C_e attributable to the decrease in h that occurs
409 when We effects are present under clinging flow conditions. Rather, Re effects appeared to be
410 dominant for these experiments. Therefore, for all of the data presented in the current study, k_h is
411 taken as 0 m. We aim to define a threshold h value below which viscous and surface tension effects
412 are significant.

413 Determining the Effect of the Varying Inclination Angle

414 Fig. 5 plots the data collected at the EFML for this study across all θ values and flow conditions
415 examined, representing Q ranging from 4.1-30.5 L/s. An attempt also was made to study the
416 flow characteristics over a model where $\theta = 20^\circ$, but sufficient free flow conditions could not be
417 achieved. Furthermore, as shown in Table 1, the maximum value of h/p for most experiments
418 was approximately unity before the flow became inundated. This was due to the bed elevation

419 remaining constant downstream of the weir. This $h/p = 1$ limit for free flow was earlier predicted
420 by Rehbock (1929) for channels where there is no drop in bed elevation downstream of the crest.
421 HHLab data are shown in Fig. 6, representing Q ranging from 10.7-84.1 L/s. In these plots, C_e
422 is calculated exactly as in Eq. (8), with $k_b = -0.001$ m and $k_h = 0$ m. It can be seen that for the
423 linear equation representing the dimensionless head-discharge rating equation, given by the form
424 $C_e = c + m(h/p)$, both the intercept (c) and slope (m) of this line tend to increase as θ decreases.
425 This can be understood by realizing that the tilting weir is an obstruction to the flow, and the amount
426 of obstruction presented to the flow by the weir depends upon θ . Generally, the streamlines over
427 the crest become more horizontal as θ decreases and as h/p increases. Due to this reduction in the
428 contraction of the overflowing jet, less upstream potential energy, represented by h , is needed for
429 the flow to pass over the obstacle presented by the weir for a given discharge.

430 To account for this effect, we propose a transformation to the h term in a manner similar to that
431 used by Kindsvater and Carter (1957) and originally examined by Rehbock (1929). These authors
432 suggested a linear transformation of the h term to account for the presence of viscous and surface
433 tension effects at low values of h for flow over a sharp-crested weir. In a similar fashion, one can
434 understand the effect of the changing θ for flow over a tilting weir as primarily affecting the h
435 term. The magnitude of this h term, representing the amount of potential energy required to pass a
436 certain flow over the weir crest, changes in response to shifting modes of approach kinetic energy
437 dissipation and momentum transfer, as brought on by the changing θ .

438 Whereas Kindsvater and Carter (1957) used a simple linear transformation to account for viscous
439 and surface tension effects for the static sharp-crested weir, an additional nonlinear transformation
440 must be utilized for the case of the variably tilting weir due to the additional degree of freedom
441 introduced by θ . Here, the flow dynamics are influenced both by the changing value of θ and the
442 relative inertial condition as defined by h/p . In keeping with the method of calculation of C_e used
443 by Kindsvater and Carter (1957), we choose to retain the notation of h_e as it is defined by Eq. (9).
444 However, it should be noted that for this study, h and h_e were equivalent since k_h was kept as 0
445 m. The purpose of our additional proposed correction factor is to transform the h_e observed over a

446 tilting weir to the h_e that would be observed under the same discharge if the weir were completely
 447 perpendicular to the bed (i.e. $\theta = 90^\circ$) using a term we call k_θ . An example transformation of
 448 the C_e values by k_θ is shown by Fig. 7. When applied to the h_e term, the head-discharge rating
 449 equation for a tilting weir becomes:

$$450 \quad Q = C_e \frac{2}{3} \sqrt{2g} b_e (k_\theta h_e)^{3/2} \quad (12)$$

451 where $C_e = 0.602 + 0.075h/p$ from Eq. (8), and h_e and b_e are given by Eqn. (9) and Eq. (10),
 452 respectively. It should also be noted that the h/p term embedded in (12) within the C_e term has
 453 not been transformed by k_θ or k_h , but is in fact the directly measured ratio at any value of θ .

454 For determining k_θ , the most relevant length scale in this flow scenario is in the vertical because
 455 this indicates the degree to which the pressure at the crest will deviate from hydrostatic due to
 456 the vertical momentum of the flow as it navigates the weir (Castro-Orgaz and Hager 2017). So,
 457 one can reasonably expect that k_θ could be understood most parsimoniously as being a function of
 458 $\sin \theta$, as was previously identified in our dimensional analysis. Using the independently measured
 459 discharge, unique values of k_θ can be found for each observation as in Eq. 13.

$$460 \quad k_\theta = \left[\frac{Q}{C_e \frac{2}{3} \sqrt{2g} b_e h_e^{3/2}} \right]^{2/3} \quad (13)$$

461 For each experiment shown in Table 1, the average value of k_θ calculated by Eq. 13 was found
 462 and is given in Table 2. Then, a trial and error best-fit regression analysis was performed to fit
 463 an empirical function to the calibrated k_θ values. Gaussian, sum of sine, and power function fits
 464 were examined. The greatest agreement with the observed k_θ values in Table 2 was found using a
 465 two-term power function, which is given by Eq. 14.

$$466 \quad k_\theta \simeq -\beta(\sin \theta)^\lambda + (1 + \beta) \quad (14)$$

467 where for the current experimental data $\beta = 0.07$ and $\lambda = 4.5$. Eq. (14) is valid for $\theta = 25^\circ - 90^\circ$,

468 with RMSE = 0.0094 (see Fig. 8).

469 Eq. 14 is monotonic in the range of realistic θ values for tilting weirs. The implicit assumption
470 in this approach is that the effect of the inclination on the contraction coefficient of the nappe is
471 continuous, and that there is no intermediate value of θ between 0-90° which represents either
472 a local maxima or minima in the discharge capacity for the tilting weir. This is an assumption
473 supported by the hypothesis of (Rouse 1932) that the effect of increasing θ on the contraction
474 coefficient would be akin to a decrease in h/p . As can be seen from Eq. 8 and Fig. 4, the influence
475 of h/p on the discharge capacity of the weir also is monotonic.

476 The inclusion of the exponent λ on the $\sin \theta$ term indicates that the effect of θ on the contraction
477 of the streamlines around the crest is nonlinear. This is likely due to the separation zone that
478 is present at higher values of θ , but eventually disappears below some threshold value. From a
479 cursory analysis of Fig. 8, a first approximation of this threshold value can be given as $\theta \approx 60^\circ$.
480 Zerihun (2022) also identified a similar threshold value of θ for the influence of the separation
481 zone on the flow dynamics. From the construction of Eq. 14, it is evident that when $\theta = 90^\circ$, k_θ
482 will be unity in Eq. (14), and Eq. (12) reduces to the classical sharp-crested weir rating equation
483 given by Kindsvater and Carter (1957). At a minimum value of $\theta = 20^\circ$, a maximum k_θ value of
484 approximately 1.07 is applied to the head term. Physically, this means that the same discharge is
485 passing over the structure inclined at $\theta = 20^\circ$ with a 6.5 % reduction in h compared to that discharge
486 passing over a sharp-crested weir inclined at $\theta = 90^\circ$.

487 **Analyzing Uncertainty and Considering Operational Constraints**

488 In addition to the 392 free-flow depth-discharge observations shown in Table 1, 48 additional
489 observations across θ values were made, but were excluded from the calibration of Eq. (14)
490 since these observations were made outside the normal operating regime of the tilting weir. This
491 concerned flows at low values of h that were subject to scale effects due to viscosity and surface
492 tension. Flows outside the normal operating regime were identified either visually by the presence
493 of a clinging nappe, or by regression analysis. If the inclusion of a certain data point at a low value
494 of h noticeably reduced the regression coefficient of the linear C_e vs. h/p equation shown in Figs.

5 and 6, it was excluded. These additional observations are included in Figs. 9 and 10 to show the influence of scale effects on the accuracy of the rating equation to predict discharge.

Fig. 9 shows a plot of C_e versus h/p computed from Eq. (12) for the 440 observed sets of Q , h , h/p and θ , in comparison to Eq. (8). In Fig. 10, $\%error$ is defined as the relative percent difference between the observed discharge during experimentation (Q_{obs}) and the predicted discharge (Q_{pred}) given by Eq. (12):

$$\%error = \frac{Q_{obs} - Q_{pred}}{Q_{obs}} \times 100 \quad (15)$$

It can be seen from Fig. 9 that there is a general relationship between h/p and $\%error$, with $h/p = 0.6$ being an approximate divergence point below which $\%error$ begins to grow. This value was previously identified by a separate study as an indicator of the lower threshold for the normal operating regime of a sharp-crested weir (Sinclair et al. 2022). For all observations of the current study, when $h/p \leq 0.6$, the mean of $|\%error|$ is 1.75%. When $h/p > 0.6$, this value is reduced to 1.15%.

To explore thresholds related to Re and We scale effects, we also define updated Re and We numbers, where the length scale has been corrected by k_θ :

$$Re_\theta = \frac{\sqrt{g}(k_\theta h)^{3/2}}{\nu} \quad (16)$$

$$We_\theta = \frac{\rho g (k_\theta h)^2}{\sigma} \quad (17)$$

Figure 10 and Table 3 reveal the relationship between Re_θ , We_θ , and the relative percent error ($\%error$) between the predicted and observed discharge for the 440 observations within the current study. Two flow regimes were identified. The threshold values of Re_θ and We_θ were identified by determining when the MAPE for the lower regime grew beyond 2 %, and the prediction bias, represented by the mean value of $\%error$, was as close to zero as possible for the upper regime. We choose $\pm 2\%$ as a somewhat arbitrary threshold, but this level of accuracy can generally be considered as excellent for flow measurements over hydraulic structures (Replogle 2002).

519 Regime I occurs when $Re_\theta \leq 3 \times 10^4$ & $We_\theta \leq 3 \times 10^2$ and represent flows that occur below
520 the absolute minimum required inertial state in the approach for the weir to be considered operating
521 in free flow. Below this threshold, scale effects cannot be justifiably neglected. Fig. 10 and Table
522 3 show that for the majority of points, this results in the observed discharge being smaller than
523 what is predicted for this regime, indicating that Re_θ effects were more significant here than those
524 due to We_θ . This can be most readily explained by understanding that as viscous effects become
525 more significant at low values of Re_θ , the piezometric head (h) must grow larger to account for the
526 decrease in the velocity head. Regime II occurs when $Re_\theta > 3 \times 10^4$ & $We_\theta > 3 \times 10^2$. Here,
527 scale effects are minimized and the accuracy of the head-discharge equation is optimized. This
528 represents the ideal operating regime for a tilting weir. Table 3 shows that for this regime, the
529 average $\%_{error}$ is only -0.08 %, indicating the bias in the predicted discharge has been removed
530 compared to Regime I.

531 These threshold values for Re_θ and We_θ can also be translated to more practical values of h ,
532 if we assume common values for physical constants and the fluid properties of room-temperature
533 water (i.e. $g = 9.81 \text{ m/s}^2$; $\mu = 10^{-3} \text{ Ns/m}^2$; $\rho = 1000 \text{ kg/m}^3$; $\sigma = 0.0728 \text{ N/m}$). These
534 approximated values are shown in Table 3. Unsurprisingly, we find a similar result as [Kindsvater
535 and Carter \(1957\)](#) for the threshold value of $h \approx 0.05 \text{ m}$ as the point above which scale effects
536 can be justifiably neglected. A similar finding was also reported in [Hager \(1994\)](#), but [Ranga Raju
537 and Asawa \(1977\)](#) advocate for a higher threshold for avoiding scale effects of $h > 0.11 \text{ m}$. The
538 frequency histograms shown in Fig. 10 also can be used to estimate the probability of a certain
539 level of measurement accuracy within each regime (see Table 3).

540 DISCUSSION

541 We now turn to some qualifications for the findings of the current study. First, it can be observed
542 from the residuals in Fig. 8 that the greatest uncertainty in the the value of k_θ occurs between
543 $\theta = 45^\circ$ and 65° . We hypothesize that this is partially due to experimental error and uncertainty
544 in the aeration condition of the downstream nappe. Another possible explanation is the instability
545 of the separation zone in this region. Additionally, in Fig. 8, it can be seen that a large gap in

546 the observed k_θ values exists between the four experiments with $\theta > 60^\circ$ and the remainder of
547 the experiments. One possible explanation for this behavior could be the disappearance of the
548 separation zone below $\theta \approx 60^\circ$, which merits further exploration.

549 An analysis of Fig. 7 reveals that k_θ may be dependent on h/p as well as $\sin \theta$. This dependence
550 is observable for experiment D in Fig. 7; but a consistent dependence was not found between all
551 experiments upon further investigation. Additional experimentation to investigate the link between
552 k_θ with both h/p and $\sin \theta$ is warranted.

553 Finally, additional observations are needed for θ between 60° and 90° . The experimental data
554 of the current study is sparse in this range, where the dynamics of the separation zone are likely
555 to change most significantly. It also remains to be seen how applicable these laboratory findings
556 can be when the flow problem is scaled up and implemented in the field. Additional complexities
557 related to the amount of friction in the approach channel, the approach geometry, the impact of
558 sedimentation over time, and changes to the surface roughness of the weir plate must be considered.

559 CONCLUSIONS

560 Observations of head and steady discharge were made for 440 flow cases in two unique ex-
561 perimental facilities, over hydraulic models of tilting weirs with inclination angles ranging from
562 $\theta = 25^\circ$ to 90° . This allowed for the calibration of a head multiplication term as a function of the
563 inclination angle, given by k_θ in Eq. (14). This empirical equation accounts for the fact that at
564 a constant discharge, the head upstream of a tilting weir generally decreases with the inclination
565 angle, due to the improved navigability of the streamlines over the crest and reduction in non-
566 hydrostatic effects near the crest. The factor k_θ then acts to adjust the observed head over a tilting
567 weir to that expected if the weir was perpendicular to the channel bed. Then, a modified form
568 of the classical sharp-crested weir rating equation, given by Eq. (12), can be applied to predict
569 steady discharge. If the inertial state of the approach flow is kept above a threshold value of at least
570 $Re_\theta = 3 \times 10^4$ & $We_\theta = 3 \times 10^2$ ($h \approx 0.05$ m) and the nappe remains fully aerated, the tilting weir
571 can be considered within an ideal operating regime where the mean absolute value of the error
572 in the predicted discharge is only 1.3 % for the current experimental data (see Table 3). We also

573 identify an h/p value of 0.6 as a more immediately applicable threshold for the normal operating
574 regime, but note that this value will likely not hold for especially small weirs (i.e. $L < 0.1$ m).

575 The results of this study work to synthesize and expand significantly upon the current level of
576 knowledge within the literature. The most extensive experimental study to date on developing a
577 head-discharge rating equation for tilting weirs is that of [Wahlin and Replogle \(1994\)](#). The current
578 study expands on this work by developing an equation having greater continuity with previous work,
579 in that it links back to the classical empirical data for the sharp-crested weir, being applicable for
580 $25^\circ \leq \theta \leq 90^\circ$. We also offer a more parsimonious monotonic solution to correct for the effect of
581 the dynamic weir inclination angle that relies less on arbitrarily maximizing goodness-of-fit metrics
582 for the observed empirical data, and instead aims to give insight to the underlying flow dynamics.
583 In terms of calibration accuracy, the current study contains a much larger number of observations
584 of the flow at θ between 45° and 90° than in previous studies. As shown by Fig. 11, this results in
585 the data from the current study agreeing well with the findings of previous researchers for certain
586 values of θ , while also being able to more fully reveal the nature of the relationship between Q_θ/Q_{90}
587 and θ across a wide range of operational θ values. In summary, the findings of this study promote
588 the tilting weir as a practical and versatile structure not only for stage regulation but also for flow
589 measurement, giving operators of open-channel flows the opportunity for much greater control and
590 efficiency within their system.

591 TOWARDS PRACTICAL IMPLEMENTATION

592 Step-by-step instructions taken from the approach laid out in this study for using the tilting weir
593 as a water flow measurement structure are as follows:

- 594 1. Measure the inclination angle (θ) of the weir from the horizontal and the crest elevation (p)
595 relative to the upstream channel bed.
- 596 2. Measure the depth of water flowing over the weir crest (h) at a distance of 3-4 times the
597 anticipated h , upstream from the crest location. For most accuracy, ensure $h > 0.05$ m.
- 598 3. Calculate h/p . For channels without a downstream drop in bed elevation below the crest,

- 599 h/p should remain below 1.
- 600 4. Using h/p , calculate C_e from Eq. 8.
- 601 5. Calculate h_e and b_e using the recommended values of k_h and k_b of **Kindsvater and Carter**
- 602 **(1957)**, as shown by Eqs. 9 and 10, respectively.
- 603 6. Calculate k_θ using Eq. 14. For most accuracy, ensure $25^\circ \leq \theta \leq 90^\circ$.
- 604 7. Using Eq. 12, estimate the discharge Q .

605 **APPENDIX**

606 **DATA AVAILABILITY STATEMENT**

607 All 440 head (h) and discharge (Q) measurements across all experiments are available in a

608 repository online in accordance with funder data retention policies at

609 https://efml.engr.colostate.edu/jhe_pugh_etal_2024/.

610 **ACKNOWLEDGEMENTS**

611 This work was supported by the Colorado Agricultural Experiment Station under Grant No.

612 COL00424, and the Republic of France under the Chateaubriand Fellowship in STEM. The authors

613 thank the reviewers for their constructive comments and recommendations.

614 **DISCLAIMERS**

615 The authors declare that they have no known competing financial interests or personal relation-

616 ships that could have appeared to influence the work reported in this paper.

NOTATION LIST

The following symbols are used in this paper:

θ = angle between the tilting weir and the horizontal channel bed;

\bar{U} = bulk (cross-section averaged) channel velocity [L/T];

C_d = discharge coefficient;

C_e = effective discharge coefficient;

b_e = effective crest length as corrected by k_b [L];

h_e = effective head as corrected by k_h [L];

p = elevation of the weir crest above the channel bed [L];

Q_θ/Q_{90} = flow amplification factor

ρ = fluid density [M/L³];

μ = fluid dynamic viscosity [M/LT];

σ = fluid surface tension [M/T²];

Fr = Froude number;

g = gravitational acceleration constant [L/T²];

α = kinetic energy correction factor;

β = k_θ Eq. empirical coefficient 1;

λ = k_θ Eq. empirical coefficient 2;

b = length of weir crest [L];

k_b = linear weir crest length correction term [L];

k_h = linear head correction term [L];

c = linear intercept;

m = linear slope;

k_θ = nonlinear head multiplication factor;

h = piezometric head above the weir crest [L];

Re = Reynolds number;

Re_θ = θ -adjusted Reynolds number;

620
621
622
623
624
625
626
627
628
629
630
631
632
633
634
635
636
637
638
639
640

continued from previous page:

- H = total hydraulic head above the weir crest [L];
- q = unit discharge per weir crest length [L^2/T];
- u = velocity of a jet issuing from a small orifice [L/T];
- L = vertical height of weir when perpendicular [L];
- Q = volumetric discharge [L^3/T];
- We = Weber number;
- We_θ = θ -adjusted Weber number;

SUPPLEMENTAL MATERIALS

REFERENCES

Abou Seida, M. and Quaraishi, A. (1976). “A flow equation for submerged rectangular weirs..” *Proceedings of the Institution of Civil Engineers*, 61(4), 685–696 Publisher: ICE Publishing.

Bazin, H. E. (1898). *Expériences nouvelles sur l’écoulement en déversoir [New Experiments on Weir Flow]*. Annales des ponts et chaussées [Annals of bridges and roads], Paris, France.

Bijankhan, M. and Ferro, V. (2017). “Dimensional analysis and stage-discharge relationship for weirs: A review.” *Journal of Agricultural Engineering*, 48(1), 1–11 Publisher: Page Press Publications.

Bijankhan, M. and Ferro, V. (2018). “Experimental Study and Numerical Simulation of Inclined Rectangular Weirs.” *Journal of Irrigation and Drainage Engineering*, 144(7), 04018012 Publisher: American Society of Civil Engineers (ASCE).

Bijankhan, M. and Ferro, V. (2020). “Experimental Modeling of Submerged Pivot Weir.” *Journal of Irrigation and Drainage Engineering*, 146(3), 04020001 Publisher: American Society of Civil Engineers.

Bos, M. G. (1976). *Discharge Measurement Structures*. International Institute for Land Reclamation and Improvement, Wageningen, The Netherlands.

Castro-Orgaz, O. and Hager, W. H. (2017). *Non-hydrostatic free surface flows*. Advances in geophysical and environmental mechanics and mathematics. Springer, Cham, Switzerland.

641 Clemmens, A., Wahl, T., Bos, M., and Replogle, J. (2001). *Water measurement with flumes*
642 *and weirs*. International Institute for Land Reclamation and Improvement, Wageningen, The
643 Netherlands ISBN: 907075455X.

644 Ferro, V. (2012). “New Theoretical Solution of the Stage-Discharge Relationship for Sharp-Crested
645 and Broad Weirs.” *Journal of Irrigation and Drainage Engineering*, 138(3), 257–265 Publisher:
646 American Society of Civil Engineers (ASCE).

647 Floodlist News (2017). “UK City of Leeds Installs Innovative Moveable Weirs FloodList.”
648 *Floodlist*, <<https://floodlist.com/protection/leeds-flood-alleviation-moveable-weirs>> (April).

649 Hager, W. H. (1994). “Dammüberfälle [Dam Overfalls].” *Wasser und Boden [Water and Land]*,
650 46(2), 33–36 Place: Heidelberg Publisher: Springer.

651 Hajimirzaie, S. M. and González-Castro, J. A. (2021). “Discussion of Experimental Modeling of
652 Submerged Pivot Weir by M. Bijankhan and V. Ferro.” *Journal of Irrigation and Drainage*
653 *Engineering*, 147(1), 07020012 Publisher: American Society of Civil Engineers.

654 Horton, R. E. (1906). *Weir experiments, coefficients, and formulas*, Vol. 16. US Government
655 Printing Office.

656 Johnson, M. C. (1996). “Discharge coefficient scale effects analysis for weirs.” Ph.D thesis, Utah
657 State University, Logan, Utah. ISBN: 9780591027167.

658 Kandaswamy, P. K. and Rouse, H. (1957). “Characteristics of Flow over Terminal Weirs and
659 Sills.” *Journal of the Hydraulics Division*, 83(4), 1345–13 Publisher: American Society of Civil
660 Engineers.

661 Khalili Shayan, H., Aminpour, Y., Peysokhan, P., and Bayrami, M. (2018). “Discussion of Extraction
662 of the Flow Rate Equation under Free and Submerged Flow Conditions in Pivot Weirs with
663 Different Side Contractions by N. Sheikh Rezazadeh Nikou, M. J. Monem, and K. Safavi.”
664 *Journal of Irrigation and Drainage Engineering*, 144(4), 07018008.

665 Khatamipour, B., Kavianpour, M. R., Khosrojerdi, A., and Ghodsi Hassanabad, M. (2022). “Nu-
666 merical Study of Flow Characteristics Over Pivot Weirs.” *Journal of Hydraulic Structures*, 8(3),
667 17–32 Publisher: Shahid Chamran University of Ahvaz.

668 Kindsvater, C. E. and Carter, R. W. (1957). “Discharge Characteristics of Rectangular Thin-Plate
669 Weirs.” *Journal of the Hydraulics Division*, 83(6), 1453–36 Publisher: American Society of
670 Civil Engineers.

671 Lee, K. S. (2016). “Analysis of submerged flow characteristics of the improved-pneumatic-movable
672 weir through the laboratory experiments.” *Journal of Korea Water Resources Association*, 49(7),
673 615–623 Publisher: Korea Water Resources Association.

674 Lee, K. S. (2018). “Experimental analysis of the sedimentation processes by variation of standing
675 angle in the improved-pneumatic-movable weir.” *Journal of Korea Water Resources Association*,
676 51(9), 795–802 Publisher: Korea Water Resources Association.

677 Lee, K.-S., Jang, C.-L., Lee, N., and Ahn, S. (2014). “Analysis of Flow Characteristics of the
678 Improved-Pneumatic-Movable Weir through the Laboratory Experiments.” *Journal of Korea
679 Water Resources Association*, 47, 1007–1015.

680 Mahdavi, A. and Shahkarami, N. (2020). “SPH Analysis of Free Surface Flow over Pivot Weirs.”
681 *KSCE Journal of Civil Engineering*, 24(4), 1183–1194 Publisher: Springer Verlag.

682 Martínez, J., Reza, J., Morillas, M. T., and López, J. G. (2005). “Design and Calibration of a
683 Compound Sharp-Crested Weir.” *Journal of Hydraulic Engineering*, 131(2), 112–116 Publisher:
684 American Society of Civil Engineers.

685 Nikou, N. S. R., Monem, M. J., and Safavi, K. (2016). “Extraction of the Flow Rate Equation under
686 Free and Submerged Flow Conditions in Pivot Weirs with Different Side Contractions.” *Journal
687 of Irrigation and Drainage Engineering*, 142(8), 04016025 Publisher: American Society of Civil
688 Engineers (ASCE).

689 Prakash, M. N. S., Ananthayya, M. B., and Kovoov, G. M. (2011). “Inclined Rectangular Weir-Flow
690 Modeling.” *Earth Science India*, 4(2), 57–67.

691 Rafter, G. W. (1900). “On the Flow of Water Over Dams.” *Transactions of the American Society of
692 Civil Engineers*, 44(2), 220–314 Publisher: American Society of Civil Engineers.

693 Rajaratnam, N. and Muralidhar, D. (1971). “Pressure And Velocity Distribution For Sharp-Crested
694 Weirs.” *Journal of Hydraulic Research*, 9(2), 241–248.

695 Ramamurthy, A. S., Tim, U. S., and Rao, M. V. J. (1987). “Flow Over Sharp Crested Plate Weirs.”
696 *Journal of Irrigation and Drainage Engineering*, 113(2), 163–172 Publisher: American Society
697 of Civil Engineers.

698 Ranga Raju, K. G. and Asawa, G. L. (1977). “Viscosity and surface tension effects on weir flow.”
699 *Journal of the Hydraulics Division*, 103(10), 1227–1231 Publisher: American Society of Civil
700 Engineers.

701 Rao, N. S. L. (1975). “Theory of Weirs.” *Advances in Hydrosience*, V. T. Chow, ed., Vol. 10,
702 Elsevier, 309–406.

703 Rehbock, T. (1929). “Discussion of Precise Weir Measurements.” *Transactions of the American*
704 *Society of Civil Engineers*, 93(1), 1143–1162 Publisher: American Society of Civil Engineers.

705 Replogle, J. A. (2002). “Some Observations on Irrigation Flow Measurements at the End of the
706 Millennium.” *Applied Engineering in Agriculture*, 18(1), 47– Publisher: American Society of
707 Agricultural and Biological Engineers.

708 Rouse, H. (1932). “The distribution of hydraulic energy in weir flow with relation to spillway
709 design.” M.S. thesis, Massachusetts Institute of Technology, Cambridge, Massachusetts.

710 Rouse, H. (1946a). “Effects of Viscosity on Fluid Motion.” *Elementary Fluid Mechanics*, John
711 Wiley and Sons Inc., New York, NY, 167–168.

712 Rouse, H. (1946b). “Pressure Variation in Accelerated Flow.” *Elementary Fluid Mechanics*, John
713 Wiley and Sons Inc., New York, NY, 57.

714 Rouse, H. and Ince, S. (1963). *History of hydraulics*. Dover Publications, New York.

715 Sarginson, E. J. (1972). “The influence of surface tension on weir flow.” *Journal of Hydraulic*
716 *Research*, 10(4), 431–446.

717 Schmocker, L., Halldórsdóttir, B. R., and Hager, W. H. (2011). “Effect of Weir Face Angles on
718 Circular-Crested Weir Flow.” *Journal of Hydraulic Engineering*, 137(6), 637–643 Publisher:
719 American Society of Civil Engineers.

720 Schoder, E. W. and Turner, K. B. (1929). “Precise Weir Measurements.” *Transactions of the*
721 *American Society of Civil Engineers*, 93(1), 999–1110 Publisher: American Society of Civil

722 Engineers.

723 Sinclair, J. M., Venayagamoorthy, S. K., and Gates, T. K. (2022). “Some Insights on Flow over
724 Sharp-Crested Weirs Using Computational Fluid Dynamics: Implications for Enhanced Flow
725 Measurement.” *Journal of Irrigation and Drainage Engineering*, 148(6), 04022011 Publisher:
726 American Society of Civil Engineers.

727 Smith, H. (1886). *Hydraulics, the flow of water through orifices over weirs, and through open
728 conduits and pipes*. Wiley, New York.

729 Stringam, B. L. and Gill, T. (2012). “Simplified Overshot Gate Constructed and Maintained by
730 Irrigation Districts.” *Irrigation and Drainage*, 61(5), 666–672.

731 Swamee, P. K. (1988). “Generalized Rectangular Weir Equations.” *Journal of Hydraulic Engineer-
732 ing*, 114(8), 945–949 Publisher: American Society of Civil Engineers.

733 USBR (1948). “Boulder Canyon project : final reports. Bulletin 3: "Studies of Crests for Over-
734 fall Dams"." *Report No. 6: Hydraulic Investigations*, United States Bureau of Reclamation,
735 Department of the Interior, Denver, Colo.

736 Wahlin, B. T. and Replogle, J. A. (1994). “Flow Measurement Using An Overshot Gate.” *Report
737 No. 1*, United States Bureau of Reclamation.

738 Zerihun, Y. T. (2022). “Free-flow discharge characteristics of an overshot gate: A non-hydrostatic
739 numerical modeling approach.” *Acta hydrotechnica*, 35(63), 101–115.

740 Zhang, X., Yuan, L., Peng, R., and Chen, Z. (2010). “Hydraulic Relations for Clinging Flow of
741 Sharp-Crested Weir.” *Journal of Hydraulic Engineering*, 136(6), 385–390 Publisher: American
742 Society of Civil Engineers.

743
744
745
746
747
748
749
750
751
752

List of Tables

- 1 Description of experimental data collected. The number in parentheses after the number of observations per experiment (n) indicates the number of points used to calibrate the free-flow head-discharge equation. The range of h/p , Re_θ , and We_θ given for each experiment constitute the cases that were considered as free flow and used to calibrate the stage-discharge equation. 32
- 2 Mean and standard deviation values of k_θ distributions for each experiment. 33
- 3 Relationship between head-discharge equation prediction accuracy and inertial regimes as defined by Re_θ and We_θ . For use as a best practice guide for the normal operating regimes of tilting weirs. 34

TABLE 1. Description of experimental data collected. The number in parentheses after the number of observations per experiment (n) indicates the number of points used to calibrate the free-flow head-discharge equation. The range of h/p , Re_θ , and We_θ given for each experiment constitute the cases that were considered as free flow and used to calibrate the stage-discharge equation.

	Location	$\theta(^{\circ})$	p (mm)	n	h/p		Re_θ		We_θ	
					min.	max.	min.	max.	min.	max.
A	EFML	25.7	65.0	27 (22)	0.50	0.94	2.0E+04	5.2E+04	1.6E+02	5.7E+02
B		29.1	73.0	26 (21)	0.57	0.91	2.9E+04	5.9E+04	2.7E+02	6.7E+02
C		36.4	89.0	36 (29)	0.36	0.98	2.0E+04	8.8E+04	1.6E+02	1.1E+03
D		45.0	106	43 (39)	0.38	0.97	2.7E+04	1.1E+05	2.4E+02	1.6E+03
E		45.0	106	23 (22)	0.43	1.05	3.3E+04	1.3E+05	3.1E+02	1.9E+03
F		50.0	115	20 (20)	0.35	0.96	2.8E+04	1.2E+05	2.5E+02	1.8E+03
G		50.0	115	27 (27)	0.34	1.02	2.6E+04	1.3E+05	2.2E+02	2.0E+03
H		53.0	120	50 (43)	0.43	0.99	3.9E+04	1.4E+05	3.9E+02	2.1E+03
I		64.0	135	27 (27)	0.32	0.99	2.9E+04	1.6E+05	2.7E+02	2.6E+03
J		71.2	142	27 (24)	0.39	0.95	4.1E+04	1.6E+05	4.2E+02	2.5E+03
K	90.0	150	27 (26)	0.24	0.93	2.2E+04	1.6E+05	1.8E+02	2.6E+03	
L	HHLab	33.0	68.6	32 (27)	0.53	1.08	2.4E+04	7.0E+04	2.1E+02	8.5E+02
M		44.0	87.5	25 (20)	0.53	0.99	3.4E+04	8.7E+04	3.3E+02	1.1E+03
N		59.0	108	28 (24)	0.41	0.88	3.0E+04	9.6E+04	2.8E+02	1.3E+03
O		90.0	126	22 (21)	0.38	0.96	3.2E+04	1.3E+05	3.0E+02	2.0E+03

TABLE 2. Mean and standard deviation values of k_θ distributions for each experiment.

Experiment	θ ($^\circ$)	$\overline{k_\theta}$	std. dev.
A	25.7	1.074	0.0081
B	29.1	1.064	0.0045
C	36.4	1.065	0.0083
D	45	1.050	0.0040
E	45	1.042	0.0040
F	50	1.064	0.0025
G	50	1.066	0.0036
H	53	1.053	0.0016
I	64	1.009	0.0047
J	71.2	1.012	0.0034
K	90	1.000	0.0022
L	33	1.055	0.0055
M	44	1.054	0.0070
N	59	1.043	0.0032
O	90	1.000	0.0038

TABLE 3. Relationship between head-discharge equation prediction accuracy and inertial regimes as defined by Re_θ and We_θ . For use as a best practice guide for the normal operating regimes of tilting weirs.

Regime	Re_θ	We_θ	$\approx h$ (cm)	n	prob. $\pm 2\%$	$\overline{\%error}$	$ \overline{\%error} $
I	$\leq 3 \times 10^4$	$\leq 3 \times 10^2$	$h \leq 5$	72	0.53	-1.45	2.08
II	$> 3 \times 10^4$	$> 3 \times 10^2$	$h > 5$	368	0.80	-0.08	1.25

List of Figures

753

754 1 Velocity magnitude vector field computed from particle-image velocimetry, with
 755 streamlines shown in blue. A zone of separated flow is apparent at the base of the
 756 weir. Flow case is from Experiment O at the HHLab; with $\theta = 90^\circ$, $p = 126$ mm,
 757 and $Q = 30$ Lps. 37

758 2 Schematic of flow over a weir. 38

759 3 Experimental setups in the Environmental Fluid Mechanics Laboratory (A.) and
 760 Hydraulic and Hydromorphology Laboratory (B), showing placement of aeration
 761 tubes downstream of the crest and the location where fresh air was supplied to the
 762 underside of the overflowing nappe. 39

763 4 Dimensionless stage-discharge plot comparing the results of the present study for a
 764 sharp-crested weir ($\theta = 90^\circ$) with the best-fit equations of previous experimentalists.
 765 Data points are calculated as $C_e = Q/\frac{2}{3}\sqrt{2g}b_e h_e^{3/2}$, with $k_b = -0.001$ m and $k_h = 0$
 766 m. The solid line corresponds to $C_e = 0.602+0.075h/p$ from Kindsvater and Carter
 767 (1957). The dashed line corresponds to $C_e = 0.602+0.082h/p$ from Rehbock (1929). 40

768 5 Dimensionless plot of C_e versus h/p for each weir inclination angle studied for the
 769 EFML experiments, with the linear best fit equation obtained from least-squares
 770 regression shown in the form: $C_e = c + m(h/p)$. Here, $C_e = Q/\frac{2}{3}\sqrt{2g}b_e h_e^{3/2}$, with
 771 $k_b = -0.001$ m and $k_h = 0$ m. Data points considered as free flow and used to
 772 calibrate the linear best fit equation are shown by circles and tallied by n . Data
 773 points excluded due to scale effects shown by 'x's'. 41

774 6 Experimental data for tilting weir flow observed at the HHLab. See Fig. 5. Here
 775 data points considered as free flow and used to calibrate the linear best fit equation
 776 are shown by triangles. 42

777	7	Example transformation of C_e values for constant h/p by way of k_θ head multi-	
778		plication factor, from Experiment D. For the original values, shown by the hollow	
779		circles, $C_e = Q/\frac{2}{3}\sqrt{2g}b_e h_e^{3/2}$, with $k_b = -0.001$ m and $k_h = 0$ m, as in Fig. 5.	
780		For the transformed values, shown by the filled circles, $C_e = Q/\frac{2}{3}\sqrt{2g}b_e(k_\theta h_e)^{3/2}$,	
781		with $k_\theta = 1.05$. Also shown is the R^2 value for the transformed values with respect	
782		to Eq. (8), given by the solid line, with $\pm 2\%$ deviation shown by the dashed lines. .	43
783	8	Empirical data and best-fit curve for the relationship between θ in degrees with the	
784		head correction factor k_θ . Mean values of k_θ are shown for each experiment with	
785		error bars representing \pm one std. dev., as in Table 2.	44
786	9	Scatter plot of C_e versus h/p for total of 440 observations after tilting weir h values	
787		have been corrected by the k_θ values given by Eq. (14). The solid line with $\pm 2\%$	
788		deviation is Eq. (8) and represents the predicted flow by Eq. (12). The Re_θ (defined	
789		by Eq. 16) colorbar is shown to indicate how the deviation from the predicted C_e	
790		to the observed grows as Re_θ decreases.	45
791	10	Top: scatter plot of 440 flow observations showing the relationship between pre-	
792		diction accuracy and Re_θ & We_θ . Bottom: frequency histograms of distribution of	
793		$\%_{error}$ for the two flow regimes identified.	46
794	11	Comparison of current and previous study results on the relative effect of the	
795		changing θ on Q for a given value of h . a) Eq. (14) of the current study, taken to	
796		the 3/2 power. Blue circles are EFML data, and red triangles are HHLab data, b)	
797		Wahlin and Replogle (1994), c) Bijankhan and Ferro (2018), and d) Hager (1994). .	47

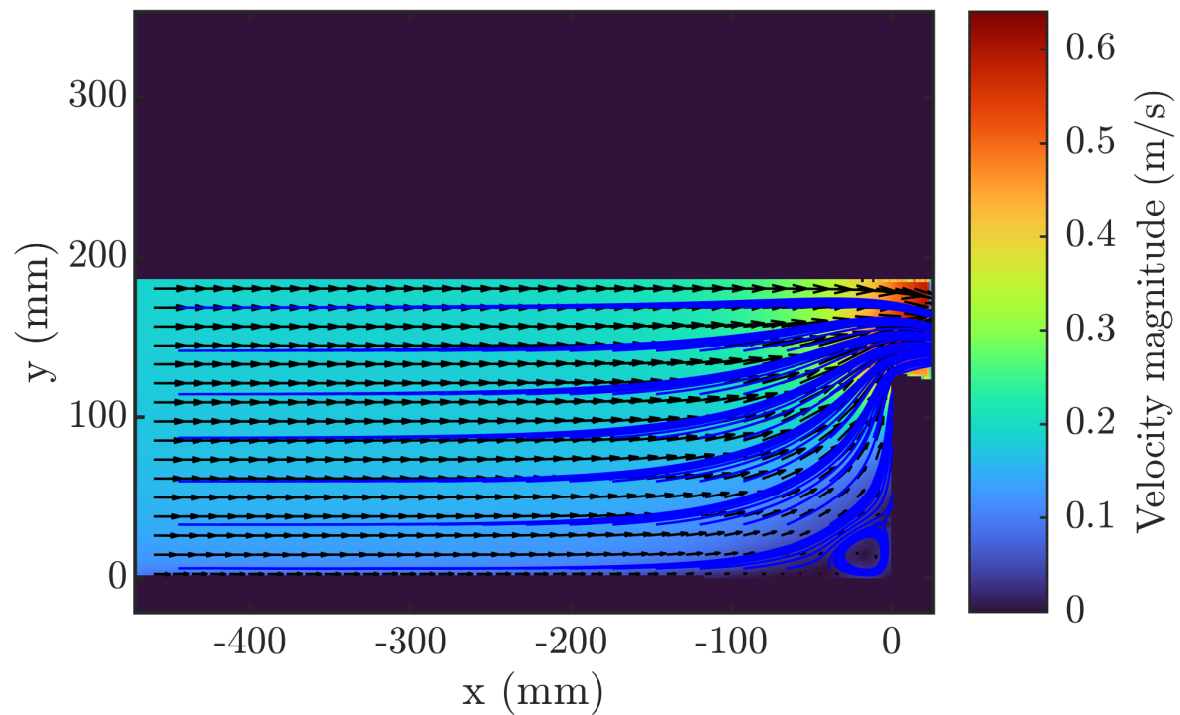


Fig. 1. Velocity magnitude vector field computed from particle-image velocimetry, with streamlines shown in blue. A zone of separated flow is apparent at the base of the weir. Flow case is from Experiment O at the HHLab; with $\theta = 90^\circ$, $p = 126$ mm, and $Q = 30$ Lps.

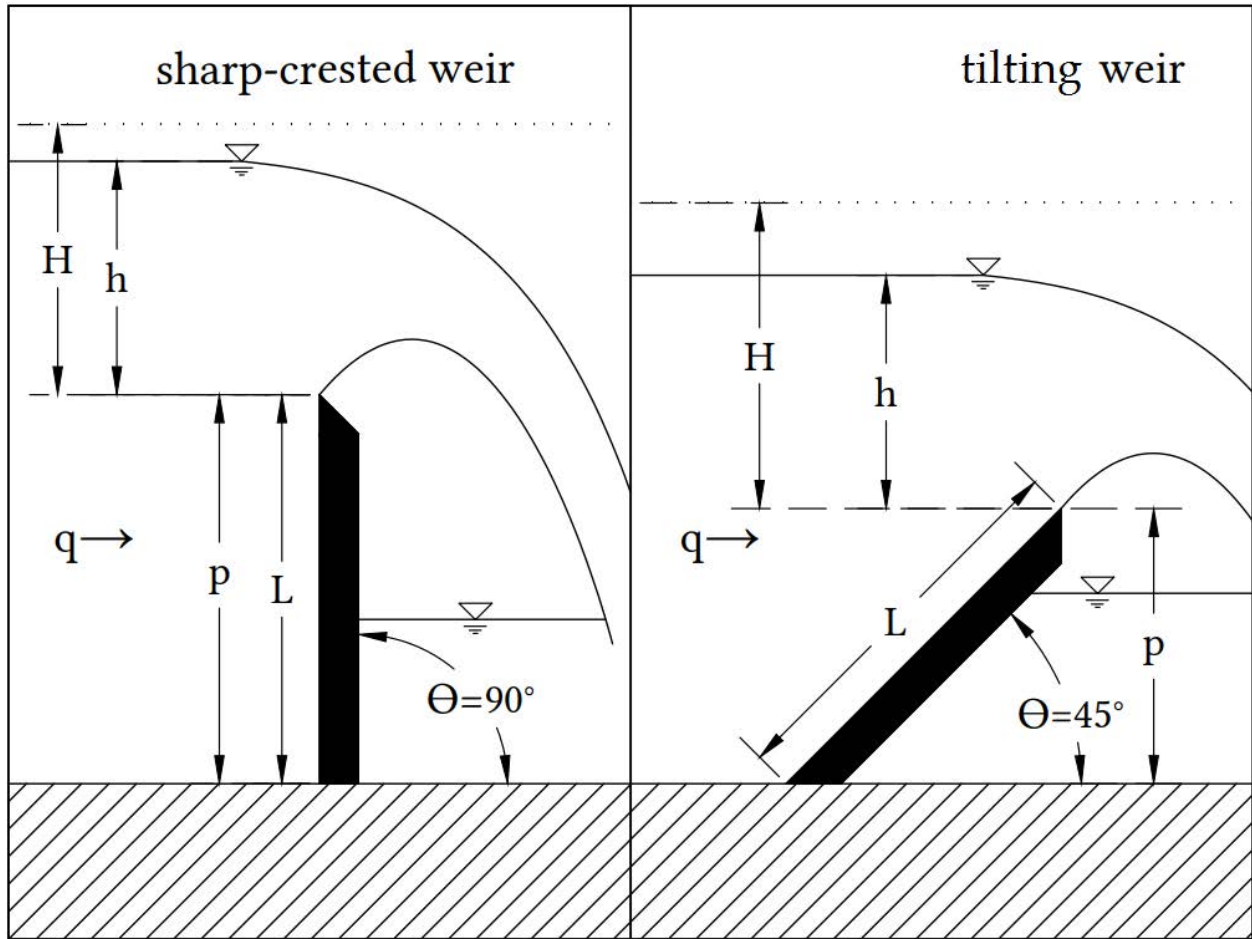


Fig. 2. Schematic of flow over a weir.

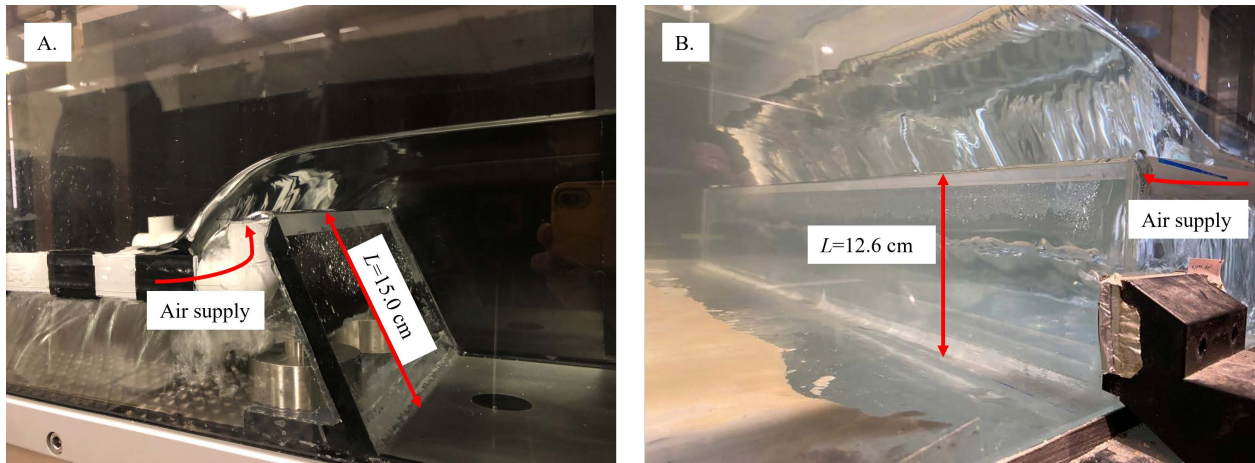


Fig. 3. Experimental setups in the Environmental Fluid Mechanics Laboratory (A.) and Hydraulic and Hydromorphology Laboratory (B), showing placement of aeration tubes downstream of the crest and the location where fresh air was supplied to the underside of the overflowing nappe.

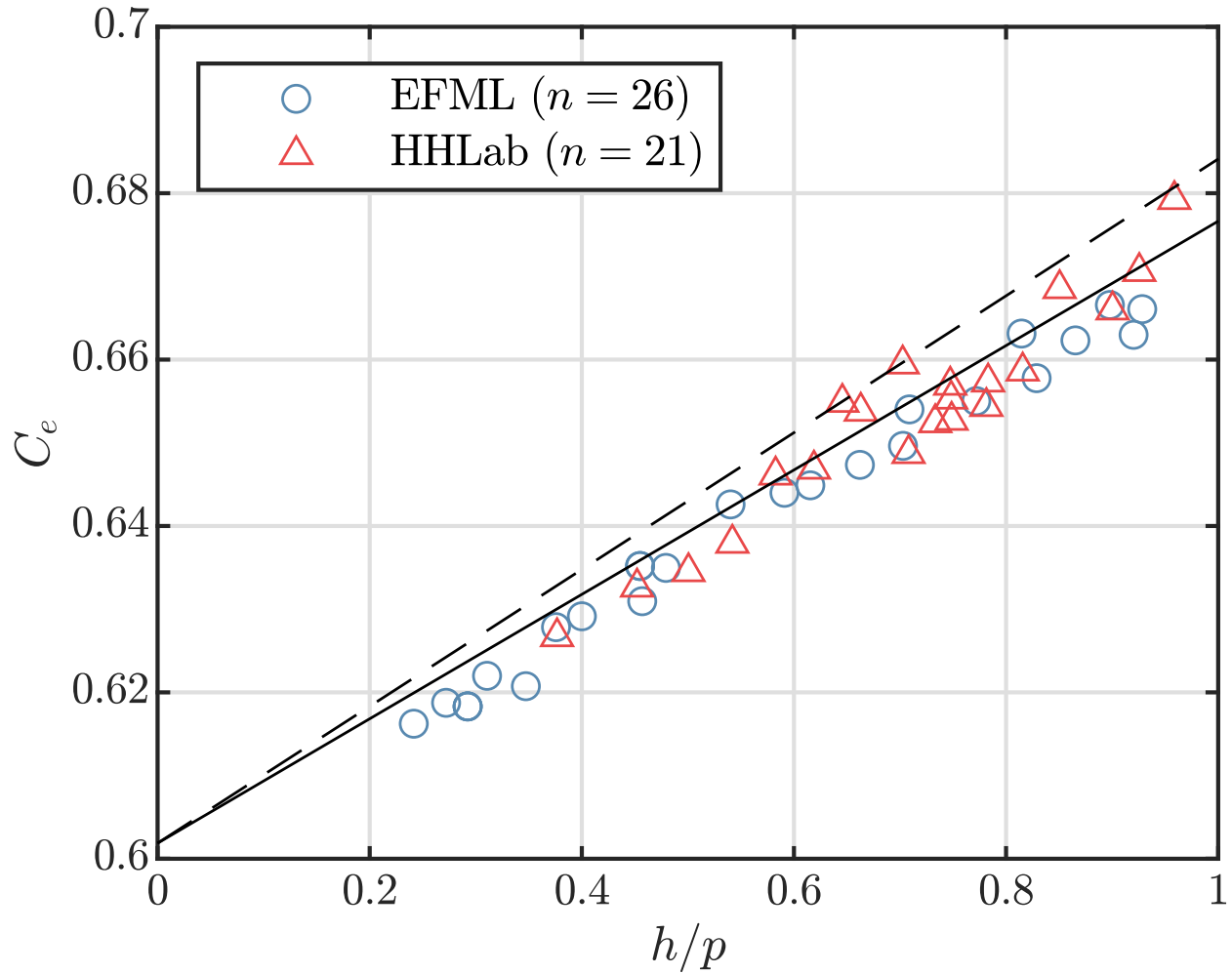


Fig. 4. Dimensionless stage-discharge plot comparing the results of the present study for a sharp-crested weir ($\theta = 90^\circ$) with the best-fit equations of previous experimentalists. Data points are calculated as $C_e = Q/\frac{2}{3}\sqrt{2gb_e}h_e^{3/2}$, with $k_b = -0.001$ m and $k_h = 0$ m. The solid line corresponds to $C_e = 0.602 + 0.075h/p$ from Kindsvater and Carter (1957). The dashed line corresponds to $C_e = 0.602 + 0.082h/p$ from Rehbock (1929).

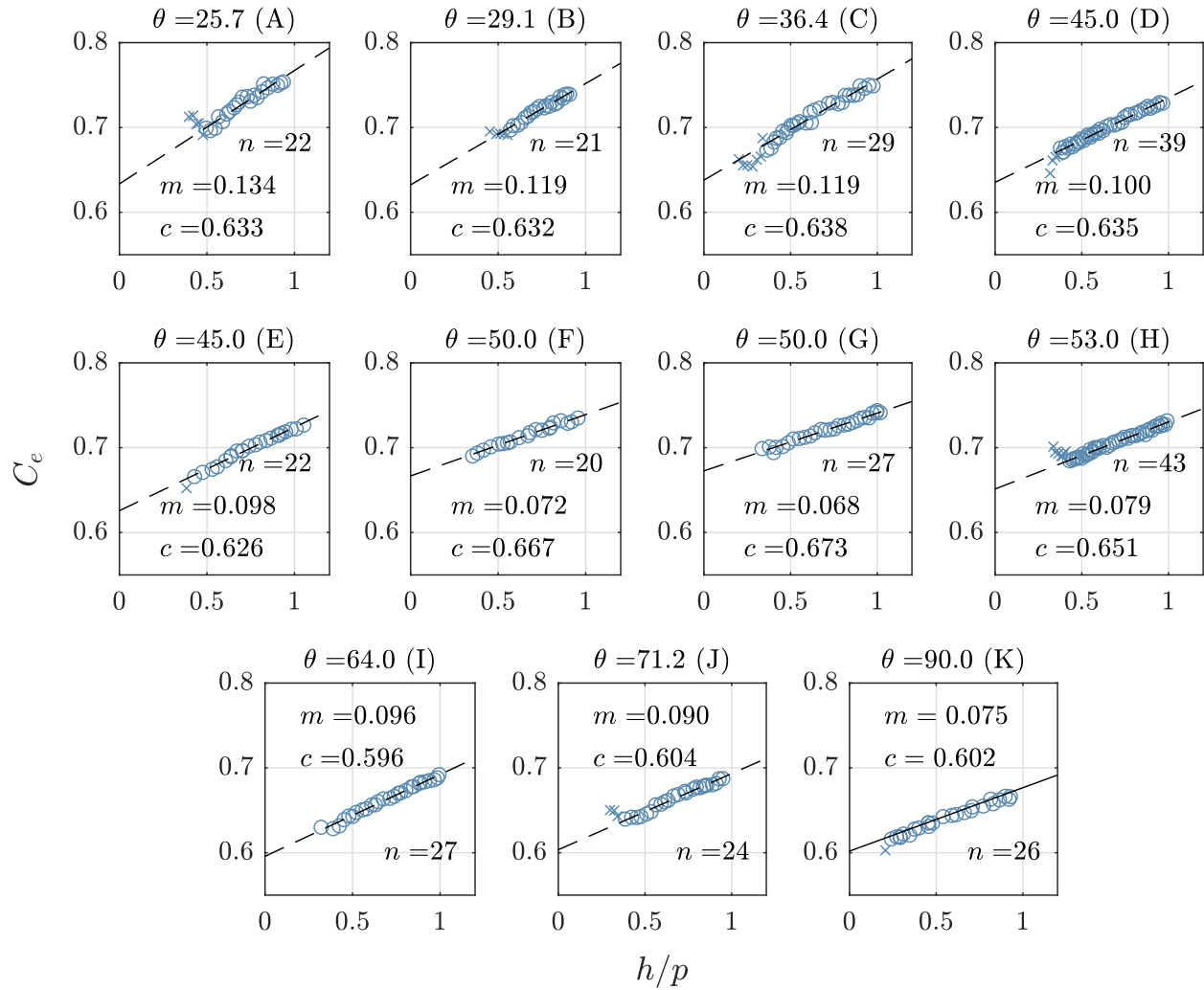


Fig. 5. Dimensionless plot of C_e versus h/p for each weir inclination angle studied for the EFML experiments, with the linear best fit equation obtained from least-squares regression shown in the form: $C_e = c + m(h/p)$. Here, $C_e = Q/\frac{2}{3}\sqrt{2gb_e h_e^{3/2}}$, with $k_b = -0.001$ m and $k_h = 0$ m. Data points considered as free flow and used to calibrate the linear best fit equation are shown by circles and tallied by n . Data points excluded due to scale effects shown by 'x's.

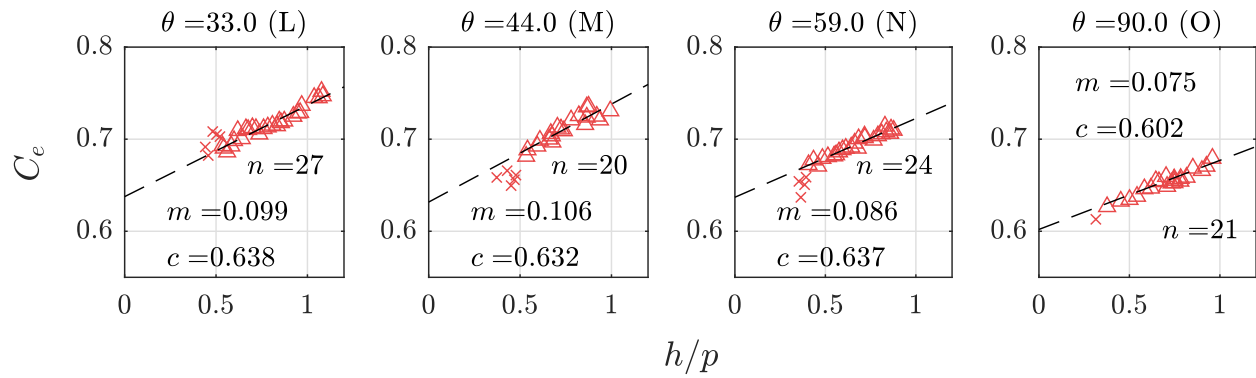


Fig. 6. Experimental data for tilting weir flow observed at the HHLab. See Fig. 5. Here data points considered as free flow and used to calibrate the linear best fit equation are shown by triangles.

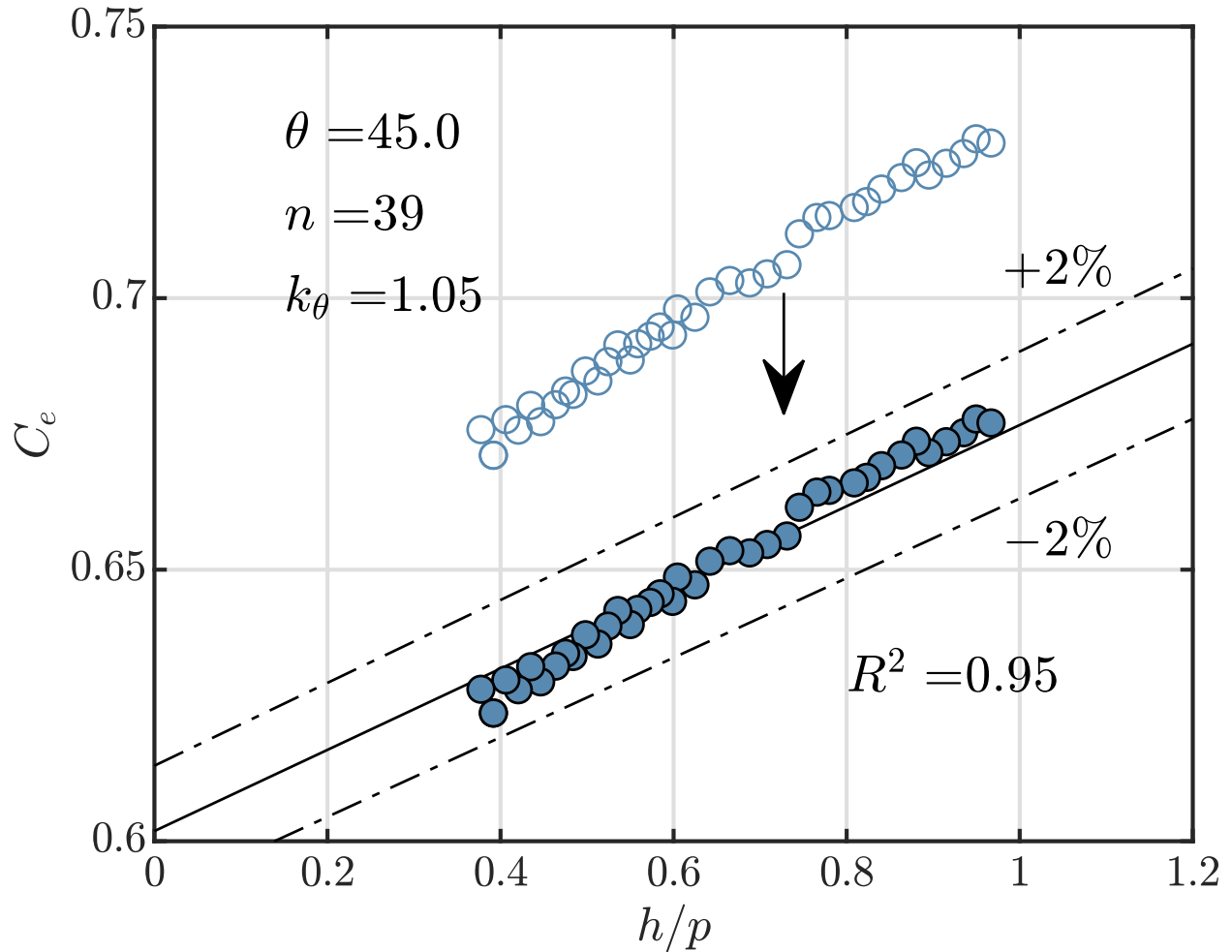


Fig. 7. Example transformation of C_e values for constant h/p by way of k_θ head multiplication factor, from Experiment D. For the original values, shown by the hollow circles, $C_e = Q/\frac{2}{3}\sqrt{2gb_e}h_e^{3/2}$, with $k_b = -0.001$ m and $k_h = 0$ m, as in Fig. 5. For the transformed values, shown by the filled circles, $C_e = Q/\frac{2}{3}\sqrt{2gb_e}(k_\theta h_e)^{3/2}$, with $k_\theta = 1.05$. Also shown is the R^2 value for the transformed values with respect to Eq. (8), given by the solid line, with $\pm 2\%$ deviation shown by the dashed lines.

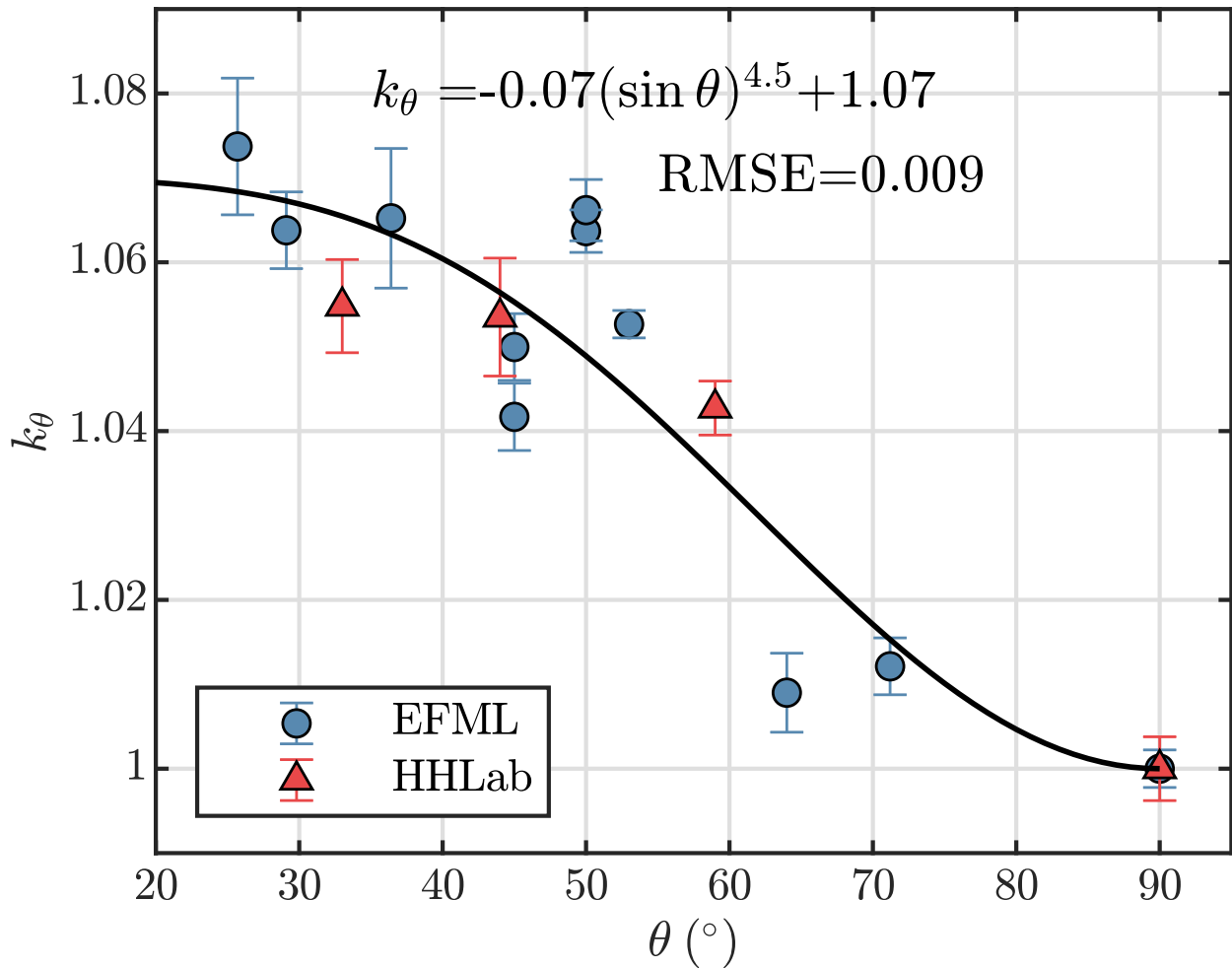


Fig. 8. Empirical data and best-fit curve for the relationship between θ in degrees with the head correction factor k_θ . Mean values of k_θ are shown for each experiment with error bars representing \pm one std. dev., as in Table 2.

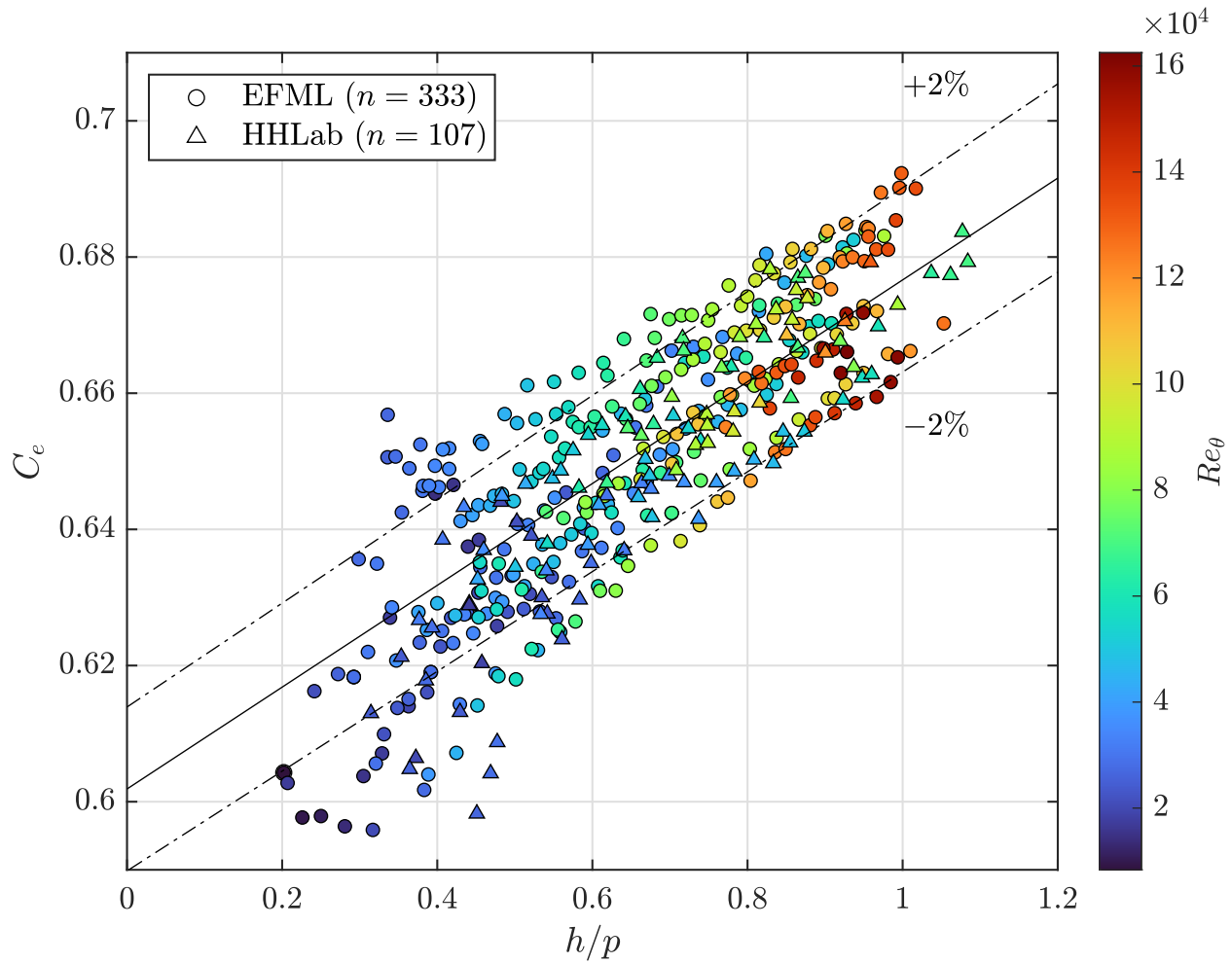


Fig. 9. Scatter plot of C_e versus h/p for total of 440 observations after tilting weir h values have been corrected by the k_θ values given by Eq. (14). The solid line with $\pm 2\%$ deviation is Eq. (8) and represents the predicted flow by Eq. (12). The Re_θ (defined by Eq. 16) colorbar is shown to indicate how the deviation from the predicted C_e to the observed grows as Re_θ decreases.

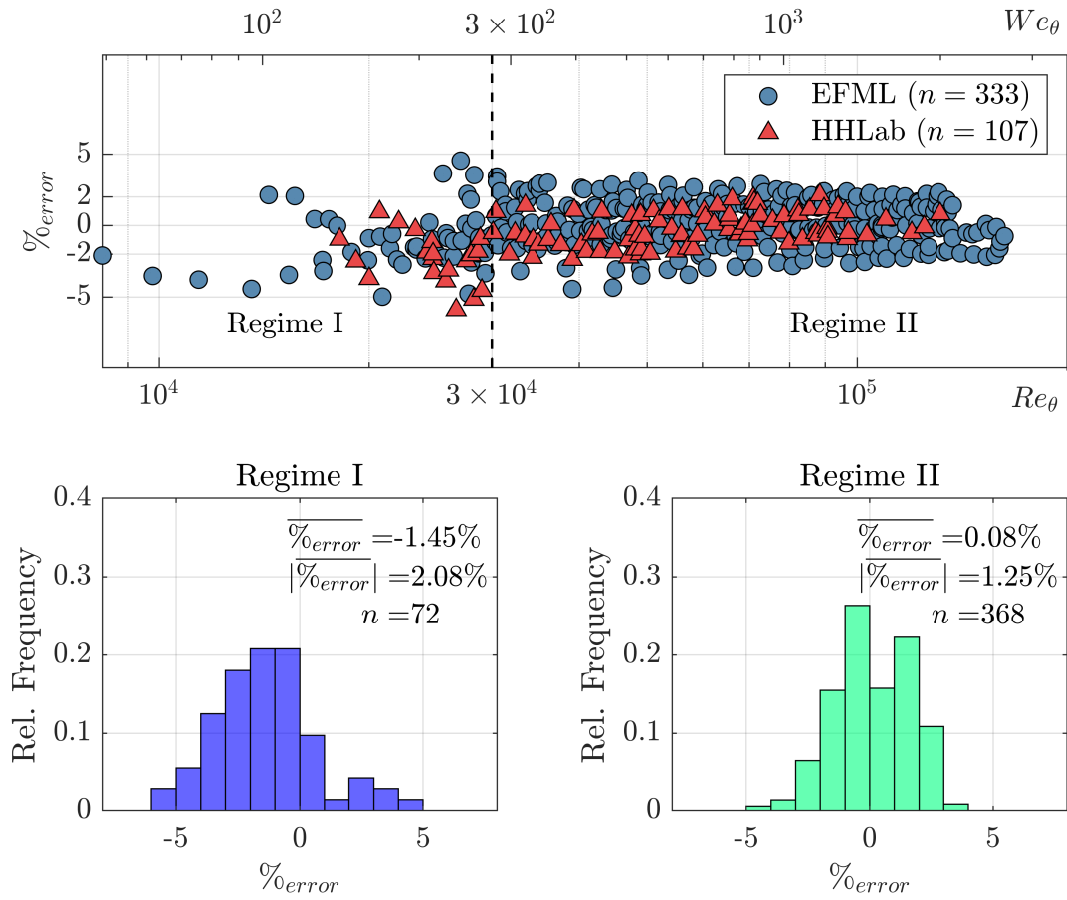


Fig. 10. Top: scatter plot of 440 flow observations showing the relationship between prediction accuracy and Re_θ & We_θ . Bottom: frequency histograms of distribution of $\%_{error}$ for the two flow regimes identified.

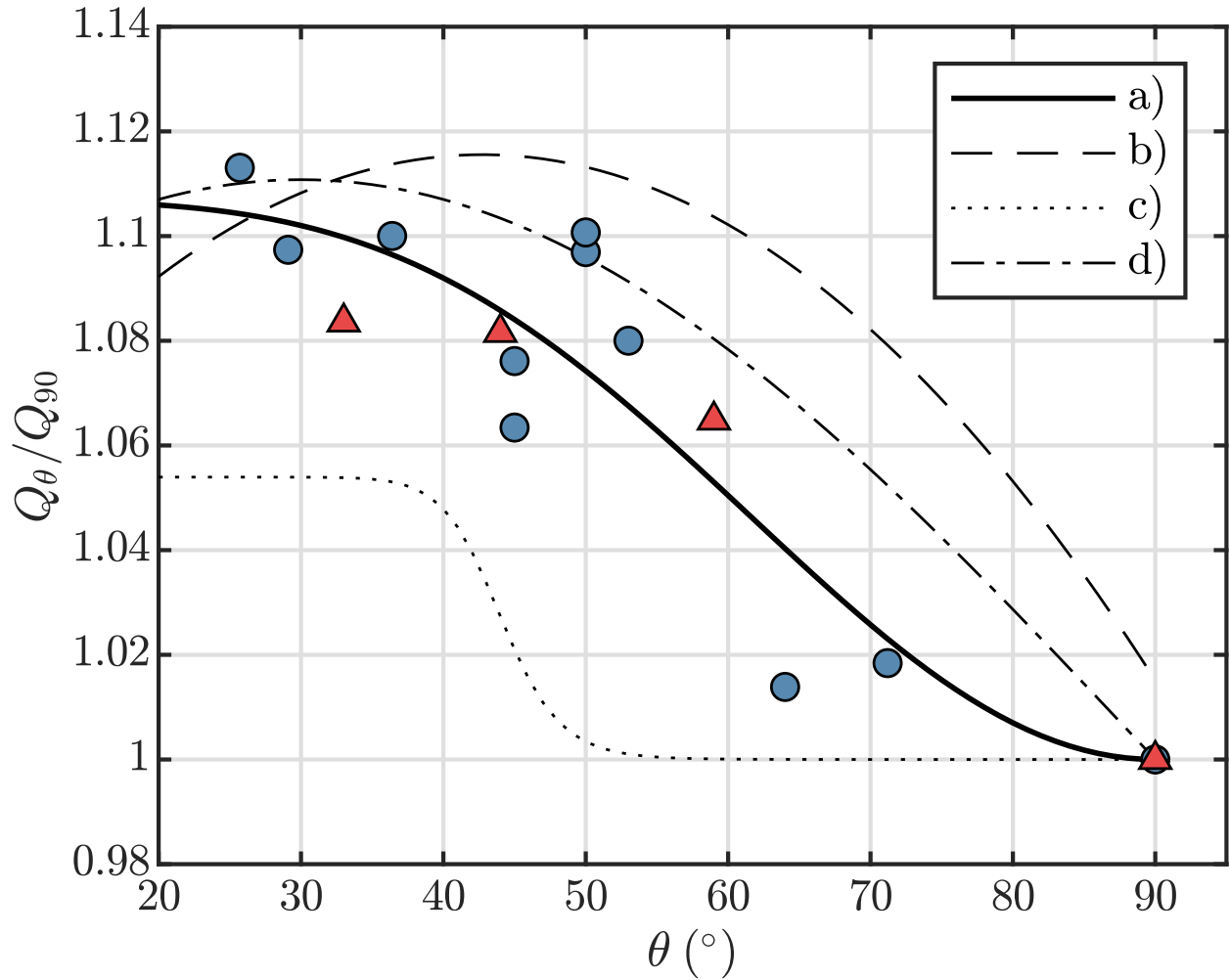


Fig. 11. Comparison of current and previous study results on the relative effect of the changing θ on Q for a given value of h . a) Eq. (14) of the current study, taken to the 3/2 power. Blue circles are EFML data, and red triangles are HHLab data, b) Wahlin and Replöge (1994), c) Bijankhan and Ferro (2018), and d) Hager (1994).